Title: Ice Shell Structure and Composition of Ocean Worlds: Insights from Accreted Ice on Earth

Authors: Natalie S. Wolfenbarger[†], Jacob J. Buffo[‡], Krista M. Soderlund[†], Donald D. Blankenship[†]

[†]Institute for Geophysics, University of Texas at Austin, Austin, TX
[‡]Dartmouth College, Hanover, NH

Corresponding Author:

Natalie S. Wolfenbarger
J.J. Pickle Research Campus
University of Texas Institute for Geophysics
10100 Burnet Road
Austin, TX, 78759-8500, USA
818-919-9930
nwolfenb@utexas.edu

Running Title: Ice Shell Structure and Composition of Ocean Worlds

Keywords: ocean worlds, ice shell, marine ice, sea ice, fractionation, salinity

Abstract: Accreted ice retains and preserves traces of the ocean from which it formed. In this work we study two classes of accreted ice found on Earth—frazil ice, which forms through crystallization within a supercooled water column, and congelation ice, which forms through directional freezing at an existing interface—and discuss where each might be found in the ice shells of ocean worlds. We focus our study on terrestrial ice formed in low temperature gradient environments (e.g., beneath ice shelves), consistent with conditions expected at the ice-ocean interfaces of Europa and Enceladus, and highlight the juxtaposition of compositional trends in relation to ice formed in higher temperature gradient environments (e.g., at the ocean surface). Observations from Antarctic sub-ice-shelf congelation and marine ice show that the purity of frazil ice can be nearly two orders of magnitude higher than congelation ice formed in the same low temperature gradient environment (~0.1% vs. ~10% of the ocean salinity). In addition, where congelation ice can maintain a planar ice-water interface on a microstructural scale, the efficiency of salt rejection is enhanced (~1% of the ocean salinity) and lattice soluble impurities such as chloride are preferentially incorporated. We conclude that an ice shell which forms by gradual thickening as its interior cools would be composed of congelation ice, whereas frazil ice will accumulate where the ice shell thins on local (rifts and basal fractures) or regional (latitudinal gradients) scales through the operation of an "ice pump".

1. Introduction

The ice shells of ocean worlds govern the feasibility of surface-ice-ocean exchange, thought to be significant for supporting habitats within the sub-ice oceans (e.g., Soderlund *et al.* 2020). The dynamic features and young surfaces of Europa and Enceladus provide compelling evidence that their subsurface oceans are continuously interacting with their overlying ice shells (e.g., Howell and Pappalardo 2018; Spencer *et al.* 2018). Because existing observations are mostly confined to

the surface, much attention has been directed towards the properties of the uppermost layer of the ice shell, where the native ice could be modified by exogenic processes (Brown and Hand 2013). Although observations of the surface provide important constraints on processes operating in the subsurface (Zolotov and Shock 2001), the properties of the subsurface itself have received less focus. Processes occurring at the ice-ocean interface, such as accretion, are likely responsible for governing and modulating bulk properties of the ice shell (Zolotov and Shock 2001; Peddinti and McNamara 2015; Buffo *et al.* 2020). Ice formed from the freezing of ocean water, referred to here as accreted ice, might serve as a fingerprint of the ocean below, recording signals of circulation (Langhorne and Robinson 1986), composition and salinity (Petrich and Eicken 2017), and potentially life (Martin and McMinn 2018).

The ice-ocean interfaces of these alien worlds and the processes that mold and shape them may be similar to those found in Earth's cryosphere. The extensive research conducted in pursuit of understanding ice on Earth represents a foundation from which to build an understanding of ice on other worlds. Previous work has leveraged sea ice as an analog to interpret surface features and connect them to processes that may be operating within Europa's ice shell (Greeley *et al.* 1998), yet these authors advised caution in drawing direct analogies between the Earth and Europa given their distinct environmental conditions. While recent works have revisited terrestrial analogs to improve our understanding of potential ice-ocean interactions on other worlds (e.g., Buffo *et al.* 2020; Schmidt 2020; Soderlund *et al.* 2020), only a small fraction of this vast and relatively untapped resource has been leveraged to date.

In this work we demonstrate that ice forming in the low temperature gradient environment beneath ice shelves can serve as a more relevant terrestrial analog than sea ice for ice forming beneath the ice shells of ocean worlds, particularly Europa and Enceladus (Section 2). We present two fundamental classes of accreted ice analogs: frazil ice and congelation ice (Section 3) and examine how their formation mechanisms influence bulk ice salinity at low temperature gradients (Section 4). We identify where each class of accreted ice might form on icy ocean worlds (Section 5), highlighting the implications for geophysical processes, bulk composition, and astrobiology (Section 6).

2. Physicochemical environments of Europa and Enceladus

The exotic appearances of the ice shells of ocean worlds can sometimes mask the more mundane reality that they are primarily composed of hexagonal water ice, the dominant ice on Earth. Furthermore, at the ice-ocean interface, where accretion of ice occurs, the physical conditions (e.g., composition, salinity, temperature, pressure) could be similar to those found in Earth's polar regions. Table 1 depicts the observational and modeled constraints on the conditions at the ice-ocean interfaces of Europa and Enceladus and demonstrates their similarity to Earth.

Table 1. Constraints on the conditions at the ice-ocean interfaces of Earth, Europa, and Enceladus from observations and models. Two possible ocean compositions are presented for Europa: (i) a sulfate-dominated ocean and (ii) a carbonate-dominated ocean. The estimates of ice thickness for Europa refer to estimates from crater and thermodynamic analyses. The pressure and temperature estimates are derived from the ice thickness ranges presented here and assume pure water ice at a density of 917 kg/m^3 and a freshwater ocean.

Parameter	Europa	Enceladus	Earth	References
Composition (Dominant Ions)	(i) SO_4^{2-}, Mg^{2+}, Na^+, Cl^- (ii) HCO_3^-, Na^+, SO_4^{2-}, Mg^{2+}	Na^+, Cl^-, HCO_3^-, CO_3^{2-}	Cl^-, Na^+, Mg^{2+}, SO_4^{2-}	Zolotov and Shock (2001); Zolotov (2007); Glein *et al.* (2015); Glein *et al.* (2018); Postberg *et al.* (2018); Daswani *et al.* (2021); Fox-Powell and Cousins (2021)
Salinity (Constrained by Geochemical Models)	12 ppt	2−20 ppt	N/A	Zolotov and Shock (2001); Zolotov (2007)
Salinity (Constrained by Observation)	>5 ppt	4−40 ppt	35 ppt	Schilling *et al.* (2007); Postberg *et al.* (2009); Hsu *et al.* (2015)
Floating Ice Thickness	3−38 km	2−50 km	0−3 km	Billings and Kattenhorn (2005); Iess *et al.* (2014); McKinnon (2015); Čadek *et al.* (2016); Čadek *et al.* (2019)
Pressure	3.6−46 MPa	0.2−5.2 MPa	0.1−27 MPa	
Pressure-Melting Temperature	269−273 K	273 K	271−273 K	

The composition and salinity of accreted ice serves as a signature of the environment in which it formed (Zolotov and Kargel 2009; Buffo *et al.* 2020). Although the compositions of the subsurface oceans on Europa and Enceladus have not been measured directly, constraints exist from theory and interpretations of data collected by both space-based and Earth-based platforms (e.g., Zolotov and Shock 2001; Postberg *et al.* 2011). Because the composition of the source water influences the properties of the ice (i.e., phase behavior governs brine volume fraction which influences thermophysical, dielectric, and mechanical properties) (Petrich and Eicken 2017), it should be considered when evaluating the relevance of terrestrial accreted ice as an analog.

Measurements of the Enceladus plume material by *Cassini* represent the only in situ observations of apparent oceanic material in the outer solar system (Glein *et al.* 2018). These observations, coupled with geochemical models (Zolotov 2007; Glein *et al.* 2015), suggest that the Enceladan ocean is highly alkaline and dominantly composed of sodium and chloride (Glein *et al.* 2018; Postberg *et al.* 2018). Assuming the plume material represents a relatively unfractionated (i.e., flash-frozen) sample of oceanic material (Fox-Powell and Cousins 2021), the salinity of the Enceladan ocean could be up to ~20 ppt—only slightly less than Earth's (~35 ppt) (Postberg et al., 2011)—although later work argues for an upper limit salinity of ~40 ppt based on the detection of silica nanoparticles in the plume material (Hsu *et al.* 2015). However, recent ocean modeling studies demonstrated that low salinity layers could be present at the ice-ocean interface

near the poles which would imply that the salinity inferred from plume material may be lower than the bulk ocean salinity (Lobo *et al.* 2021; Zeng and Jansen 2021).

Although a plume sample remains elusive for Europa, geochemical models of Europa's ocean chemistry have attempted to constrain the dominant species using observations of Europa's surface and atmosphere. For example, the Europa K1a model of Zolotov and Shock (2001) was tuned by Earth-based observations of chemical species detected in Europa's tenuous atmosphere (Brown 2001). This model suggested that Europa's ocean composition is broadly comparable to that of the Earth's, where the dominant ionic species are sulfate, magnesium, sodium, and chloride. Other geochemical models identify similar dominant species, although their relative abundance (NaCl-dominated vs. MgSO4-dominated) remains the subject of debate (Kargel *et al.* 2000; Zolotov 2008; Zolotov and Kargel 2009). Results from a more recent model suggest that a carbonate dominated Europan ocean is also possible (Daswani *et al.* 2021). Early interpretations of *Galileo* NIMS data were consistent with the presence of hydrated sulfate or carbonate salts in regions associated with resurfacing (McCord *et al.* 1998; McCord *et al.* 1999). Later analysis by Carlson *et al.* (2005) suggested that the signature could instead be attributed to hydrated sulfuric acid. This would also explain the apparent enhancement observed on the trailing hemisphere, where the surface is highly irradiated and bombarded by Iogenic sulfur. Higher spectral resolution observations acquired by Earth-based platforms were able to identify features associated with magnesium sulfate salts but found that they were confined to the trailing hemisphere and spatially correlated with sulfuric acid (Brown and Hand 2013). Brown and Hand (2013) used the spatial correlation of the magnesium sulfate with radiation products to argue that sulfate salts are a radiation product and that the ice shell and ocean are dominantly composed of chloride salts, which have no distinct spectral feature in the near-infrared. These results were supported by additional Earth-based observations, which were able to confirm that acid-dominant components were concentrated along the trailing hemisphere and salt-dominant components were associated with endogenous surface features (Fischer *et al.* 2015). Additionally, because the salt-dominant component lacked spectral features consistent with hydrated sulfate minerals, the authors proposed the spectrum may instead be associated with chloride evaporite deposits. Laboratory experiments have demonstrated that when sodium chloride is exposed to conditions similar to those expected at Europa's surface, it darkens into a color consistent with that observed across Europa's surface, particularly in features thought to be associated with material from the sub-ice ocean (Hand and Carlson 2015). Recent observations of Europa's surface with the *Hubble Space Telescope* revealed a spectral feature consistent with irradiated sodium chloride that was again highly correlated with endogenous features (Trumbo *et al.* 2019). These laboratory, Earth-based, and space-based observations collectively indicate that chloride salts are being entrained in the ice shell. Similar to the Earth and Enceladus, chloride may represent an important component of Europa's ocean composition.

Although measurements of Europa's induced magnetic field by the *Galileo* magnetometer support the existence of a global subsurface ocean; constraining the salinity of the ocean from these measurements is a challenge as the signal is a convolution of electrical conductivity and ice/ocean thicknesses. Gravitational measurements from *Galileo* flybys provide an upper limit of ~200 km to the thickness of the ice/ocean layer (Anderson *et al.* 1998). Using this thickness constraint and a minimum value of 0.7 for the normalized amplitude of the induced dipole moment relative to the primary field, Zimmer *et al.* (2000) were able to estimate a minimum

ocean conductivity of 0.072 S/m. Later work by Schilling *et al.* (2007) further constrained the parameter space to obtain a minimum conductivity of 0.5 S/m for a 100 km ocean. For terrestrial seawater at 0 °C, this translates to a practical salinity (PSS-78) of ~5. Hand and Chyba (2007) use the induced magnetic field amplitude of 0.97 obtained by Schilling *et al.* (2004) to argue for an ice shell less than 15 km thick overlying an ocean of conductivity that could range from 3 S/m (practical salinity of ~36 at 0 °C) to 23 S/m (practical salinity undefined) More recent work by Vance *et al.* (2021b) argues that the reduction in electrical conductivity with decreasing temperature could raise these salinity estimates for colder oceans associated with thicker ice shells. This suggests, because of the broad parameter space of possible ocean salinities, a valid ocean analog could span in salinity from brackish to hypersaline.

The surfaces of icy ocean worlds are directly exposed to the vacuum of space and have measured temperatures ranging from approximately 86 K to 132 K on Europa (Spencer et al., 1999) and 32 K up to 145 K on Enceladus (Spencer *et al.* 2006). At the south pole of Enceladus, the temperature approaches 200 K near a set of linear features, referred to as tiger stripes, which are spatially correlated with the plumes observed by *Cassini* and are thought to serve as a conduit to the subsurface ocean (Spencer *et al.* 2018; Hemingway *et al.* 2020). The conditions at depth, however, could be relatively mild. The equivalent of one Earth atmosphere of pressure translates to ~100 m of ice on Europa and ~1 km of ice on Enceladus (Fig. 1a). This suggests the near-vacuum conditions at the surface of these bodies becomes irrelevant at relatively shallow depths, well-below the hypothesized ice shell thicknesses of Europa and Enceladus (Table 1). The pressure ranges expected beneath these ice shells are consistent with what is expected beneath floating ice on Earth, which can be up to a few kilometers thick (Table 1, Fig. 1). The melting temperature of ice does not vary significantly with pressure for ice shell thicknesses of approximately 1 m to a few kilometers on Europa and 10 m to tens of kilometers on Enceladus. This suggests that for both Europa and Enceladus, neglecting the influence of impurities, the temperature at the ice-ocean interface is likely to be depressed by only a few degrees (~3 K beneath a 30 km ice shell on Europa, ~0.5 K beneath a 50 km ice shell on Enceladus). Note that although the influence of pressure on melting temperature is minor, it is critical to driving “ice pumps” beneath ice shelves on Earth, a basal ice redistribution process introduced and further discussed in Section 3.2. The pressure-melting temperature represents an upper limit for the temperature at the ice-ocean interface since impurities within the ocean can further reduce the equilibrium temperature.

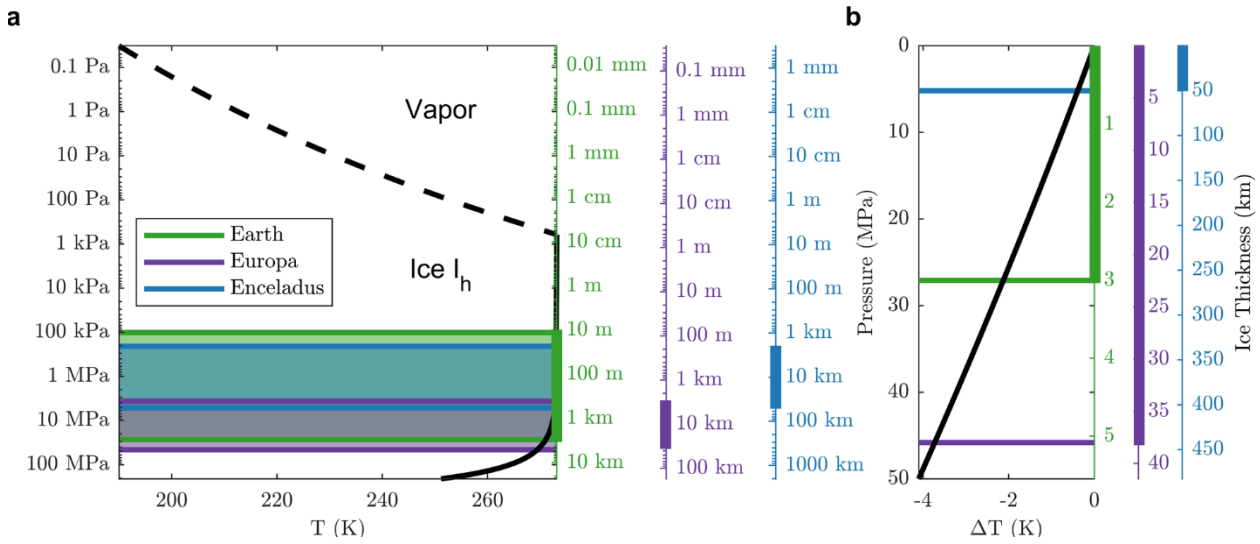

Figure 1. Pressure at the ice-ocean interface for the range of ice shell thicknesses on Earth (green axis), Europa (purple axis), and Enceladus (blue axis) represented **(a)** logarithmically across the entire stable region of ice Ih and **(b)** linearly across the range of pressures expected at the ice-ocean interfaces of these worlds. The Earth axis does not include the effect of atmospheric pressure, hence the minimum pressure-equivalent thickness of 10 m. The dashed black curve depicts the phase boundary between Ice Ih and water vapor, and the solid black curve depicts the phase boundary between Ice Ih and liquid water. The range of floating ice thickness for each body, specified in Table 1, is represented by the shaded region in (a). The colored lines depict the upper and lower bounds of ice thickness. Only the upper bound ice thickness is included in (b). The density of ice is taken to be constant at 917 kg/m^3.

Freezing point depression is a mechanism often invoked to explain the presence of liquid water in otherwise cryogenic environments (Toner *et al.* 2014; Hammond *et al.* 2018). For an ideal solution with low concentrations of impurities, freezing point depression is dependent upon the concentration of dissolved impurities, but not their composition. As the eutectic point is approached, this colligative assumption breaks down and composition becomes relevant to the freezing point depression. For the range of plausible salinities and ice shell thicknesses hypothesized for Europa, this implies the temperature at the ice-ocean interface could range from the pressure-melting point to the eutectic point of a salt solution. For a sodium chloride ocean, the maximum freezing point depression would be ~21 K at a concentration of 232 ppt (Drebushchak *et al.* 2019), whereas for a magnesium sulfate ocean, the maximum corresponds to only ~4 K at a concentration of 174 ppt (Pillay *et al.* 2005). Ammonia, initially implicated in promoting resurfacing processes at Enceladus (Squyres *et al.* 1983), can depress the freezing point of water by almost 100 K at a concentration of 354 ppt (Leliwa-Kopystyński *et al.* 2002); however, only trace amounts were detected in the Enceladus plume material (Waite *et al.* 2009; Waite *et al.* 2017; Fox-Powell and Cousins 2021). If the plume observation is representative of the concentration of ammonia within the subsurface ocean, it would amount to a freezing point depression on the order of a degree. The composition and concentration of impurities, in addition to the overburden pressure, defines where multiphase systems can exist within the ice shell (Hammond *et al.* 2018)—creating the opportunity for complex reactive transport processes

important to the habitability of these worlds (Kalousová *et al.* 2014; Buffo *et al.* 2020; Hesse *et al.* 2020).

3. **Terrestrial Accreted Ice**

Although the physicochemical environments of Europa and Enceladus may share similar characteristics to ice-ocean interfaces on Earth, a critical distinction between the ice-ocean interfaces of ocean worlds in the outer solar system and Earth involves the temporal and spatial scales of processes operating at that interface (Vance *et al.* 2021a). Timescales of freezing processes beneath the ice shells of ocean worlds are likely orders of magnitude slower than sea ice on Earth (i.e., sea ice growth occurs on seasonal cycles, whereas the ice shells of ocean worlds are potentially the product of over a hundred million years of accretion and ablation). The temperature gradient at the ice-ocean interface is an important consequence of these vastly different temporal and spatial scales. If the ice is actively thickening and in a conductive thermal regime, the temperature profile is approximately linear throughout the shell, and the magnitude of the temperature gradient is governed by the thickness of the ice layer and temperature at the surface and base of the ice layer (Thomas 2017). As such, the thick ice shells of ocean worlds are subject to lower temperature gradients and freezing rates than experienced by sea ice on Earth (Table 2). Furthermore, as the ice shell approaches equilibrium thickness, the growth rates should decrease to zero. Therefore, we consider the estimated freezing rates for Europa and Enceladus in Table 2 to represent upper bounds, which are notably an order of magnitude lower than sea ice growth rates measured on Earth. Although sea ice is one of the most ubiquitous and most studied forms of accreted ice on Earth, we propose that there are other forms of ice which may represent more relevant analogs for ice accreting at the ice-ocean interface of ocean worlds.

Table 2. Estimates of ice shell growth rates for Europa and Enceladus compared to measured sea ice growth rates on Earth. Growth rates are expressed in terms of the published units and in cm/s for direct comparison. All modeled freezing rates for Europa and Enceladus neglect the influence of salts and thus may be higher than reality.

	v	$v \times 10^6$ (cm/s)	Source
Sea Ice	0.15 – 2.29 cm/day	1.7 – 27	Souchez *et al.* (1988)
Sea Ice	0.7 – 1.7 cm/day	8.1 – 20	Nakawo and Sinha (1981)
Sea Ice	1.2 – 4.5 cm/day	14 – 52	Legendre *et al.* (1991)
Sea Ice	0.03 cm/hr – 0.38 cm/hr	8.3 – 105	Melnikov (1995)
Sea Ice (Nominal Max)	1.5 – 3 cm/day	17 – 35	Shokr and Sinha (2015)
Europa	150 km ocean freezing in 100 Myr	0.005	Pappalardo *et al.* (1998)
Europa	30 km freezing in 7×10^6 yr	0.014	Mitri and Showman (2005)
Europa	40 km ocean freezing in 30 Myr	0.004	Roberts and Nimmo (2008)
Europa	100 km ocean freezing in 62 Myr	0.005	Quick and Marsh (2015)
Europa	Increase from 5.67 km/Myr to 8.22 km/Myr due to merging of convective cells	0.018 – 0.026	Peddinti and McNamara (2019)
Europa	30 km freezing in 1.5 Myr ($\dot{\varepsilon} = 1\times10^{-10}$ s^{-1}) 5 km freezing in 165 kyr ($\dot{\varepsilon} = 3\times10^{-10}$ s^{-1})	0.063 – 0.096	Green *et al.* (2021)
Enceladus	<few mm/yr to maintain topographic anomalies	<0.01	Čadek *et al.* (2019)
Enceladus	~km/Myr freezing rate required to maintain steady state	<0.01	Kang *et al.* (2021)

Ice which accretes beneath the thick ice shelves of Antarctica forms in a significantly lower temperature gradient environment than sea ice and could approach growth velocities relevant to the ice-ocean interfaces beneath the ice shells of ocean worlds. In this work, we adopt the genetic terminology of Tison *et al.* (1998) and focus our study on two classes of accreted ice found beneath ice shelves: frazil ice and congelation ice (Fig. 2). Although naturally accreted ice is rarely composed entirely of frazil or congelation ice, these broad classifications facilitate discussions of bulk ice properties in the context of their formation mechanisms and will allow us to examine how each might influence the bulk salinity of the ice shells of ocean worlds.

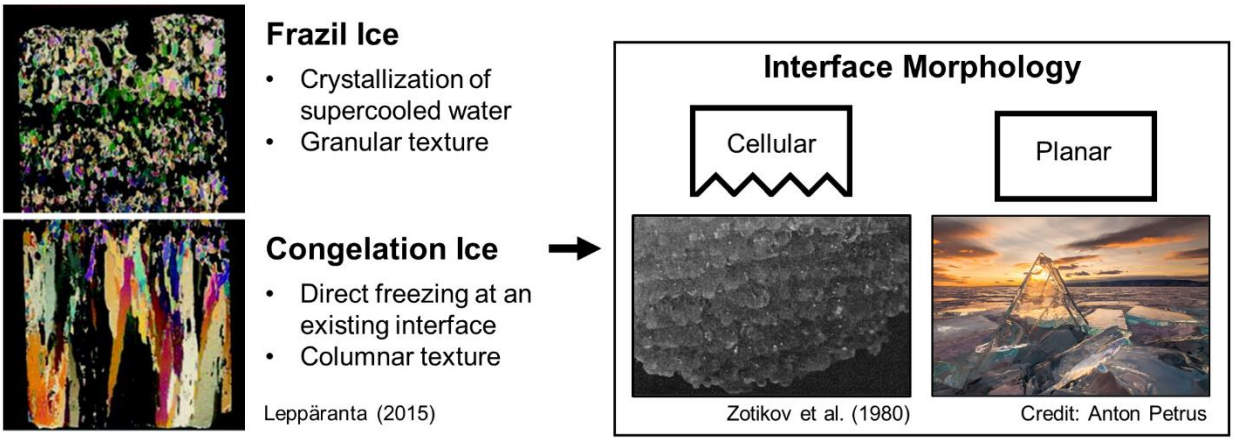

Figure 2. Genetic classification of accreted ice and characteristics of the microstructural interface morphology for congelation ice.

3.1. Frazil and Congelation Ice

Ice that crystallizes within a supercooled water column, as opposed to at a solid interface, is referred to as frazil ice. Frazil ice is formed in the presence of turbulent water which has been supercooled by tenths to hundredths of a degree (Weeks and Ackley 1986; Mager *et al.* 2013; Robinson *et al.* 2019), where increased supercooling generally promotes increased frazil production (Ettema *et al.* 1984). There are a number of mechanisms in nature that can promote supercooling and thus the production of frazil. Examples of such mechanisms include the adiabatic rise of water masses to a lower-pressure environment and double diffusion occurring between two adjacent water bodies at different temperatures and salinities (see Mager *et al.* 2013). Ice crystals formed from collisions of larger ice crystals, the refreezing of spray, or snow can serve as nucleation sites for frazil ice crystals (Osterkamp 1977). It was long believed that foreign particles, such as organic matter, could serve as nucleation sites for frazil, but no experimental or field observations have demonstrated that this is possible at the degrees of supercooling observed in nature (<1 °C) (Daly 1984; Robinson *et al.* 2019). Turbulence is also necessary to promote secondary nucleation, responsible for generating meaningful quantities of frazil crystals (Ettema *et al.* 1984). Because frazil ice forms from individual crystals which can nucleate independent of each other, it has no preferred orientation and a granular texture (Fig. 2). Once a stable frazil ice layer has formed, congelation ice growth can occur.

Congelation ice refers to ice produced by the direct freezing of water at an existing ice interface, driven by conductive heat losses (Weeks and Ackley 1986). In congelation ice, the microstructural morphology of the ice-water interface (e.g., planar, cellular, dendritic) is highly dependent on the purity of the source water and the growth velocity (Harrison and Tiller 1963; Lofgren and Weeks 1969; Wettlaufer 1992; Wettlaufer 1998). Ultimately, the microstructural morphology of the ice-ocean interface is related to the phenomenon of constitutional supercooling (Harrison and Tiller 1963; Eicken 2003), originally proposed and studied in the field of metallurgy (Rutter and Chalmers 1953; Jackson 2004). Constitutional supercooling refers to supercooling that occurs in advance of the freezing front. The role of constitutional supercooling in congelation ice growth is critical to governing its substructure and in turn its properties (Eicken 2003; Weeks 2010; Petrich and Eicken 2017). Rejection of impurities locally

enhances the concentration and depresses the freezing point at the interface, promoting supercooling ahead of the interface. If perturbations occur in the presence of constitutional supercooling, the supercooled fluid serves as a heat sink that promotes further growth, forming cells or dendrites. In the absence of this supercooled layer, small perturbations in the interface morphology are not energetically favorable and a planar interface remains stable.

Characteristics of the interface are significant to the efficiency of impurity incorporation in ice (Nagashima and Furukawa 1997). A planar interface is more efficient at rejecting impurities, whereas a cellular interface retains impurities through the entrapment of brine between cells (Osterkamp and Weber 1970; Eicken 2003; Weeks 2010; Petrich and Eicken 2017). For the growth rates typical of sea ice on Earth (Table 2), it has been demonstrated that congelation ice forming from seawater will always result in the development of a cellular interface (Wettlaufer 1992). Congelation ice is typically characterized by a columnar texture, where crystals preferentially elongate parallel to the direction of the temperature gradient (Harrison and Tiller 1963; Tison *et al.* 1998). In low salinity environments, such as freshwater lakes, constitutional supercooling during freezing is minimal and the morphology of the microstructural interface can remain planar for higher growth velocities than it would for seawater (Leppäranta 2015).

3.2. Marine Ice and Sub-Ice-Shelf Congelation Ice

Marine ice is specific to frazil ice that collects and consolidates beneath ice shelves or within ice shelf rifts characterized by a low temperature gradient environment. The formation of marine ice is generally thought to occur in two phases, defined by Tison *et al.* (2001) as (1) the frazil ice phase and (2) the consolidation phase. The frazil phase encompasses the formation and accumulation of frazil ice crystals beneath the ice shelf. These crystals preferentially form and collect where the ice draft thins rapidly—features such as inverted channels, rifts, or crevasses beneath the ice shelf (Tison *et al.* 1993; Khazendar *et al.* 2001; Khazendar and Jenkins 2003). The consolidation phase involves the buoyancy-driven compaction of accumulated frazil crystals. In this phase, crystals agglomerate and collect, forming a permeable layer. As more frazil accumulates, buoyant pressure builds up at the ice-water interface, compressing the layer and forcing out interstitial water, reducing the brine volume fraction. The bulk density of the ice-brine system is thus counter-intuitively reduced by compaction. At a certain stage in the consolidation phase, the ice becomes impermeable and any remaining brine is trapped in the ice as inclusions at triple-junctions and along grain boundaries (Moore *et al.* 1994). The final stage of consolidation involves the freezing of remaining interstitial water through congelation growth, analogous to the incorporation of frazil ice layers beneath growing sea ice known as platelet ice. Unlike platelet ice, this interstitial congelation growth occurs at a much slower rate due to the insulation from atmospheric thermal forcing by overlying glacial ice. The lower unconsolidated portion of the marine ice layer is a hydraulically connected region that can extend from tens of meters up to ~100 m from the base of the ice shelf (Craven *et al.* 2009). The formation of marine ice beneath ice shelves is part of a process that has been referred to as an “ice pump”, where the pressure dependence of the freezing point supports the operation of a continuous cycle involving the melting of ice at depth and the accretion of ice at a more shallow location (Lewis and Perkin 1986). The term marine ice is sometimes broadly applied to ice that forms beneath ice shelves. Here, however, we distinguish between marine ice and sub-ice-shelf congelation ice to emphasize the distinct formation mechanisms between these forms of accreted ice.

Because the ice-ocean interface beneath ice shelves is fairly insulated from atmospheric forcing (i.e., the ocean is shielded from frigid air temperatures by hundreds of meters of ice), the formation of congelation ice at the base of an ice shelf is rare (Fig. 4); however, it has been observed beneath certain ice shelves in Antarctica (Gow and Epstein 1972; Zotikov *et al.* 1980; Souchez *et al.* 1991). A simple model to predict the formation of congelation ice beneath an ice shelf was proposed by the Ross Ice Shelf Project (RISP) and summarized by Neal (1979). When water at the pressure-melting temperature flows in the direction of increasing ice shelf thickness, it must dissipate heat to remain at the pressure-melting temperature. Under conditions where the thickness gradient and flow speed are such that the sensible heat conduction to the overlying ice layer exceeds that which must be dissipated at the boundary layer to maintain the pressure-melting temperature, bottom freezing will occur (Neal 1979). The J-9 Ross Ice Shelf core represents a unique and valuable sample of congelation ice acquired at a depth of ~400 m within a zone of bottom freezing (Zotikov *et al.* 1980). The published sample is uniquely well-characterized for sub-ice-shelf congelation ice and includes measurements of salinity, grain size, texture, and freezing rate. The freezing rate estimate was obtained from an observed transition in growth conditions at the bottom 2 cm, which was attributed to localized melting caused by a drilling expedition the prior year (Zotikov *et al.* 1980). The estimate was validated by a simple heat transfer calculation (Zotikov *et al.* 1980) and represents the only estimate of sub-ice-shelf congelation ice growth rate obtained through direct inspection of a sample of the basal accreted ice. Congelation ice can also form beneath ice shelves experiencing high rates of surface ablation (e.g., locations with strong katabatic winds) (Souchez *et al.* 1991).

4. **Salinity of Accreted Ice from Experiments and Ice Cores**

We review published studies characterizing the bulk salinity of accreted ice to develop an understanding for how salt entrainment processes might scale to the ice shells of ocean worlds. As ice forms, salts are rejected from the crystal lattice to the grain boundaries as brine. Select impurities, specifically chloride, fluoride, ammonium, and acids (H+), are soluble within the ice lattice and are accommodated as defects within the ice crystal. The total concentration of salts in ice, including both those accommodated within the lattice and those along grain boundaries, is referred to as the bulk salinity (Hunke *et al.* 2011). Because the efficiency of salt entrainment in ice is correlated to the ice growth velocity, we explore relationships modeling the bulk salinity of ice as a function of growth velocity and show that only salt entrainment in the slowest growth velocity regime is relevant to the bulk salinity of the ice shells of Europa and Enceladus. We then focus our study on ice cores collected in environments which represent ice-ocean accretion within this regime.

4.1. Congelation Ice across Growth Regimes

The partitioning of salt into ice, S_{ice}, from ocean water of salinity, S_0, can be represented by the effective solute distribution coefficient, $k(v) = S_{ice}/S_0$, which is a function of ice growth velocity (Burton *et al.* 1953; Weeks and Lofgren 1967). Although models for the effective solute distribution coefficient do not directly represent the physics of sea ice desalination as it is understood today (Notz and Worster 2009), existing models fit the data well for both natural and artificial ice over a range of freezing rates relevant to sea ice (Fig. 3). Parameterizations of salt partitioning based on growth velocity represent a computationally inexpensive approach to

augment simple freezing models that do not directly model ice desalination processes. Furthermore, representing the salinity of ice as a fraction of ocean salinity allows salt entrainment in ice to be parameterized independent of the source water salinity. Even though more complex numerical models of ice desalination processes exist (Griewank and Notz 2013; Buffo *et al.* 2018; Wells *et al.* 2019), effective solute distribution coefficients are invaluable for certain planetary applications where high resolution salinity profiles are not needed and properties of the ocean are poorly constrained.

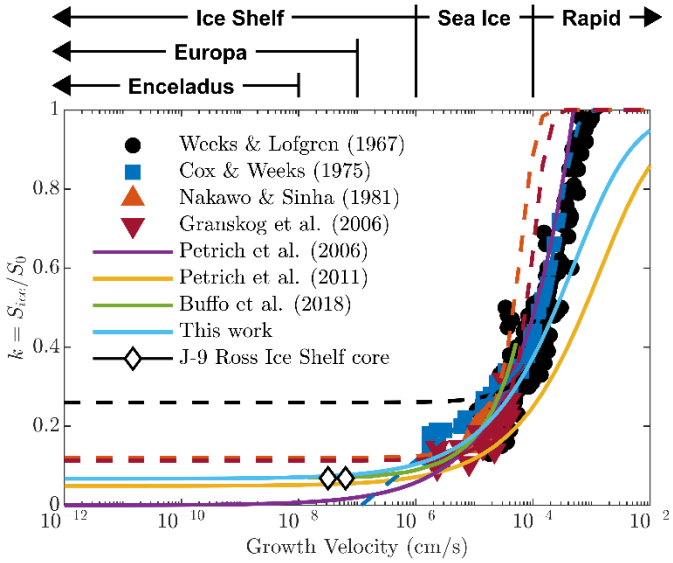

Figure 3. Summary of relationships representing the effective solute distribution coefficient, $k = S_{ice}/S_0$, as a function of ice growth velocity. The markers represent data points from experimental or field data. Solid lines through data points represent least squares fits of the data to published models for the solute distribution coefficient, where dashed lines represent extensions of the model beyond the available data range. The green curve is a smoothed representation of multiple runs of the mushy-layer model of Buffo *et al.* (2018), assuming a critical porosity inferred from the salinity of the J-9 core from Ross Ice Shelf, Antarctica. The light blue curve represents the model presented in Eq. 1.

At growth velocities above those naturally occurring on Earth (Fig. 3), ice experiences minimal fractionation ($k \approx 1$) upon freezing, implying that it serves as a relatively unaltered chemical fingerprint of the source water. This rapid freezing regime would include processes occurring at or near the surface at Europa and Enceladus such as the flash freezing of brine infiltrating porous ice at the surface or plume material which is frozen as it ascends through the fractured ice shell from a subsurface reservoir below (McCord *et al.* 2002; Schmidt *et al.* 2011; Thomas *et al.* 2017; Fox-Powell and Cousins 2021). Published measurements of sea ice growth rates span from approximately ~1×10^{-6} to 1×10^{-4} cm/s (Table 2). Salt partitioning in this regime has been characterized using both natural (Nakawo and Sinha 1981; Granskog *et al.* 2006) and artificial (Weeks and Lofgren 1967; Cox and Weeks 1975) samples of congelation ice. Studies of natural sea ice samples are more challenging due to the difficulties in obtaining samples and the uncertainties in natural growth rates. The dataset of Nakawo and Sinha (1981) is particularly

valuable because of the high sampling frequency of ice salinity and temperature they obtained over the growth season that produced nearly continuous profiles of ice salinity and growth rate. Although growth velocities for the sea ice regime and above are not directly applicable to accretion occurring at the ice-ocean interface of ocean worlds (Fig. 3), it represents the regime where the effective solute distribution coefficient is most sensitive to growth velocity and where more significant variations in bulk ice shell salinity might occur.

At a certain stage in growth, the salinity profile of the ice no longer evolves in time due to progressive brine drainage. This salinity has been referred to as the stable salinity (Nakawo and Sinha 1981; Petrich *et al.* 2006) or steady-state salinity (Petrich *et al.* 2011). The natural congelation ice samples of Nakawo and Sinha (1981) in Fig. 3 are thought to be representative of this stable salinity and as such fall below the experimental data, which was not given sufficient time to reach this steady-state condition. The Baltic sea ice samples of Granskog *et al.* (2006) in Fig. 3 represent the stable salinity of ice formed from a lower salinity source water. These data suggest that a lower salinity source water may enhance the efficiency of salt rejection, possibly due to a change in interface morphology (Granskog *et al.* 2006). Their data are consistent with those of Weeks and Lofgren (1967), which included samples formed from low salinity source waters.

Because salt in ice is predominantly trapped interstitially as brine, the steady-state salinity is thought to be coupled to a critical porosity (~5%) below which ice is thought to be impermeable to brine transport (Golden *et al.* 1998; Golden *et al.* 2007). The critical porosity is typically a prescribed parameter in numerical models of sea ice desalination (Petrich *et al.* 2011; Griewank and Notz 2013; Buffo *et al.* 2018; Wells *et al.* 2019; Buffo *et al.* 2020) and governs the finite ice salinity that the model asymptotically approaches as the growth velocity approaches zero (i.e., the system reaches equilibrium) (Fig. 3). The distribution coefficient associated with this limit has been referred to as the effective equilibrium distribution coefficient, k_{eq} (Burton *et al.* 1953; Weeks and Lofgren 1967) and would represent the bulk salinity of congelation ice as the growth velocity approaches zero. Other sea ice desalination models do not explicitly impose a critical porosity, but instead use permeability-porosity relationships that represent a percolation threshold as a significant reduction in permeability which occurs as the critical porosity is approached (Petrich *et al.* 2006; Buffo *et al.* 2021). Figure 3 demonstrates that at the growth velocities predicted for the ice shells of ocean worlds, the effective equilibrium solute distribution coefficient should govern the bulk salinity of the ice shell.

4.2. Low Temperature Gradient Accreted Ice

For ocean worlds, we are interested in the accretion of ice in low temperature gradient environments characterized by growth velocities within the ice shelf regime ($< 10^{-6}$ cm/s), where $k \approx k_{eq}$ (Fig. 3). Because experimental studies cannot sample this growth velocity regime, we must leverage Earth's natural laboratory to estimate the salinity of ice formed in these environments. We present a survey of the available published ice core data from Antarctica and the Arctic, including samples of marine ice and sub-ice-shelf congelation ice (Fig. 4). We provide characteristics of the environment in which the ice formed, including depth from the surface as a proxy for temperature gradient (i.e., deeper ice implying a lower temperature gradient) and estimates of growth velocity where available. We also include properties of the ice

such as salinity and $\delta^{18}O$ where known, which can serve as a proxy for modification of the seawater by glacial meltwater (i.e., values close to 2‰ implying minimal modification). $\delta^{18}O$ is often used to determine the origin of the ice (i.e., marine or meteoric) when the salinity signal is ambiguous (Gow and Epstein 1972; Morgan 1972; Oerter *et al.* 1992). Estimates for the effective solute distribution coefficient were obtained by dividing the ice salinity by the salinity of seawater, assumed to be 35 ppt. Although it represents a relevant analog, we exclude the ice core from Lake Vostok because the mechanism of accretion remains debated, and the properties of the lake water are not well constrained (Souchez *et al.* 2000; Souchez *et al.* 2004; Lipenkov *et al.* 2015). Table 3 presents the values of k_{eq} estimated from selected ice cores in Fig. 4. We discuss how these values are obtained in the following sections.

Location	Site Description	Name	Type	Depth from Surface (m)	Salinity (ppt)	$\delta^{18}O$ (ppt)	k	Growth Velocity (cm/s)	Source(s)
Amery Ice Shelf	Suture Zones	G1	M	270 – 315	0.05 – 0.1	0 – 2	10^{-3}	1×10^{-6}	Morgan (1972)
		AM01	M	276 –376	0.03 – 0.56	2	10^{-4} –10^{-3}	~10^{-6}	Craven et al. (2004, 2009)
Roi Baudouin Ice Shelf	Rift Exposed at Surface	D	M	10 – 20	0.3 – 9	2	10^{-2} – 10^{-1}	-	Pattyn et al. (2012)
		E	M	0 – 15	0.3 – 2	2	10^{-3} – 10^{-2}		
Filchner-Ronne Ice Shelf	Thin Region beyond Henry Ice Rise	B13	M	152.8 – 215	0.02 – 0.1	2	10^{-4} – 10^{-3}	4×10^{-6}	Oerter et al. (1992) Eicken et al. (1994)
Ross Ice Shelf	Region of Heat Loss to the Ice Shelf	J-9	SISC	410 – 416	2 – 4	-	10^{-3} – 10^{-2}	~10^{-8}	Zotikov et al. (1980)
McMurdo Ice Shelf	Exposed at Surface near Minna Bluff	Site 3	M	0 – 5	0.115	2.3	10^{-3}	-	Fitzsimons et al. (2012)
		C5	M	0 – 2.65	0.26 ± 0.11	1.63 ± 0.24	10^{-3}	-	Koch et al. (2015)
		C9	M	0 – 3.04	0.20 ± 0.15	1.64 ± 0.43	10^{-3}		
		C15	M	0 – 9.44	0.29 ± 0.18	0.47 ± 0.48	10^{-3}		
Dailey Islands	Exposed at Ice Shelf Surface	No. 1	M	0 – 6.74	0.01 – 0.09	-	10^{-4} – 10^{-3}	-	Gow et al. (1965)
		No. 2	M	0 – 15.25	0.01 – 0.05	-	10^{-4} – 10^{-3}		
Koettlitz Glacier Tongue	Exposed at Surface of Glacier Tongue	1	SISC	0 – 12.8	0.2 – 3.76	2.51 – 1.61	10^{-3} – 10^{-1}	-	Gow and Epstein (1972)
		3		0 – 13	2.19 – 5.26	1.76 – 1.85	10^{-2} – 10^{-1}		
Nansen Ice Shelf	Exposed in Rift at Ice Shelf Surface	NIS	M	0 – 45	0.005 – 0.19	1.80 – 2.37	10^{-4} – 10^{-3}	2×10^{-6}	Khazendar et al. (2001) Tison et al. (2001) Khazendar et al. (2003)
Hells Gate Ice Shelf	Exposed at Ice Shelf Surface	Granular	M	0 – 1.5	0.016 – 0.081	2 – 3.5	10^{-4} – 10^{-3}	3×10^{-7}	Souchez et al. (1991)
		Columnar	SISC	0 – 1.5	1.6 – 2.6	1 – 2	10^{-2}		
		Platelet	M	0 – 1.5	0.24 – 0.49	2 – 3.5	10^{-3} – 10^{-2}		
Arctic	"Ice Island"	SP-6	SISC	0 – 9	0 – 3	-	10^{-2}	-	Cherepanov (1964)
	Sea Ice	9a	CS	0 – 1.5	4 – 7.5	-	10^{-1}	~10^{-5}	Nakawo and Sinha (1981)

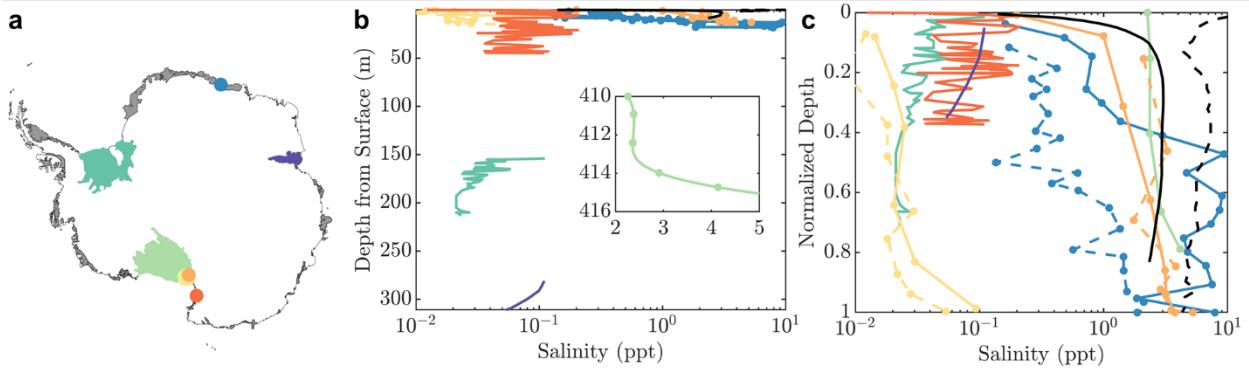

Figure 4. A summary of properties and characteristics of terrestrial accreted ice from published ice core data. The first two columns specify the location where the ice core was collected and a

description of the sample site. The sites are color and texture coded by ice shelf and presented in the map of Antarctica in **(a)**. Where multiple cores were collected from a single location, the second core is represented as dashed. The third column provides the name of the ice core or ice type as referenced in the sources in the rightmost column. The type of accreted ice is specified in the fourth column according to the following codes: M (Marine Ice), SISC (Sub-Ice-Shelf Congelation Ice), CS (Congelation Sea Ice). The plots representing the **(b)** absolute and **(c)** depth-normalized salinity profiles follow the same color and texture coding represented in the table and map. The plots represent data from the published works referenced in the rightmost column.

Table 3. Equilibrium distribution coefficients inferred from published samples of natural accreted ice from Earth. Values were derived using the minimum salinity observed in the core and an ocean salinity of 35 ppt. Where a trend (either increasing or decreasing) was absent in the salinity profile, the mean salinity was adopted instead. Only ice cores where melt water did not appear to contribute significantly to the salinity signal (i.e. $\delta^{18}O \approx 2$ in Fig. 4) were included. Ice type follows the same coding presented in Fig. 4 (SISC: Sub-Ice-Shelf Congelation Ice, M: Marine Ice).

k_{eq}	Ice Type	Sample	Source
6.71E-02	SISC	J-9 Ross Ice Shelf core	Zotikov *et al.* (1980)
6.46E-02 – 6.71E-02	SISC	Ice Island SP-6 core	Cherepanov (1964)
6.29E-02	SISC	Ice Island SP-4 core	Cherepanov (1964)
1.43E-03	M	AM01 Amery Ice Shelf core	Morgan (1972)
6.86E-04	M	B13 Filchner-Ronne Ice Shelf core	Moore *et al.* (1994)
5.71E-03	M	C9 McMurdo Ice Shelf core	Koch *et al.* (2015)
1.71E-03	M	Nansen Ice Shelf core	Tison *et al.* (2001)
4.57E-04	M	Granular ice from Hells Gate Ice Shelf	Souchez *et al.* (1991)

4.2.1. Sub-Ice-Shelf Congelation Ice

Samples of congelation ice formed in low temperature gradient environments are limited (Fig. 4). Unlike sea ice, where growth velocities can be estimated by periodic measurements over the growth season (Nakawo and Sinha 1981), estimates of growth velocity for congelation ice beneath ice shelves are obtained using models. Certain ice cores collected from ice shelves in Antarctica (Ross Ice Shelf, Koettlitz Glacier Tongue, Hells Gate Ice Shelf) were observed to have the columnar texture indicative of congelation ice (Gow and Epstein 1972; Zotikov *et al.* 1980; Souchez *et al.* 1991). Published estimates of the growth velocities associated with accreted ice found beneath ice shelves (Fig. 4) are well within the asymptotic growth velocity regime of the models in Fig. 3. Because of its extensive thickness, the sea ice island SP-6 likely approaches temperature gradients within this regime and is thus also classified as sub-ice-shelf congelation

ice (Fig. 4). The salinity of accreted ice at these low temperature gradients can thus be used to estimate k_{eq} for congelation ice (Table 2).

The bottom 2 cm of the Ross Ice Shelf core was described to have a "waffle-like" texture (Fig. 2), consistent with an actively growing congelation ice layer (Zotikov *et al.* 1980), often referred to as a "skeletal layer" (Buffo *et al.* 2020). The salinity profile reveals a transition at approximately 2 m above the ice-ocean interface from constant to monotonically increasing with depth (Fig. 4b). In sea ice, an increase in salinity with depth near the base is recognized to be a feature of growing sea ice (Eicken 1992). The increasing salinity observed near the base of the Ross Ice Shelf core and the description of the basal texture suggest the bottom 2 m of the Ross Ice Shelf core is in a state of active desalination. However, the constant salinity observed above this transition can be considered the stable salinity, attained at growth rates within the asymptotic regime (Fig. 3, 4), and can thus be used to obtain an estimate of k_{eq} (Table 2). The salinity profiles associated with the Koettlitz Glacier Tongue ice cores do not appear to have achieved a stable salinity, particularly the ice sampled from Hole 3 (Fig. 4c). This interpretation is supported by samples of seawater obtained from the bottom of Hole 3, which was found to be enriched in salt, suggesting the ice in this location is also actively desalinating (Gow and Epstein 1972). Additionally, the $\delta^{18}O$ signal shows slight modification of the ice source water by glacial meltwater. These observations suggest that the Koettlitz Glacier Tongue ice cores may not be representative of an equilibrium state of salt partitioning, although the salinity profile of Hole 1 suggests a stable salinity could fall between 2 and 3 ppt which is in-family with the Ross Ice Shelf core. A salinity profile is not available for the Hells Gate Ice Shelf columnar ice (Souchez *et al.* 1991); however, the $\delta^{18}O$ signal presents with some evidence of modification by glacial meltwater. Therefore, we adopt the maximum observed salinity to estimate a value for k_{eq}. The salinity profile associated with Ice Island SP-6 drops off sharply near the ice-atmosphere interface (Fig. 4c) which is indicative of post-genetic brine redistribution (Eicken 1992). As such, for SP-6, we adopt the salinity at the base and the mean salinity to estimate bounds on k_{eq}. The equilibrium distribution coefficients derived from these congelation cores are similar to one another and on the order of 10^{-2} (Table 2). Of the sub-ice-shelf congelation cores considered here, the salinity profile associated with the Ross Ice Shelf core shows the least evidence of post-genetic desalination or brine redistribution. The stable salinity of this ice core is representative of the effective equilibrium solute distribution coefficient for natural congelation ice, $k_{eq} = 6.7 \times 10^{-2}$, which is the same value inferred for the upper bound of the SP-6 core (Table 2). Notably, this value is similar to the critical porosity of 5% for sea ice discussed in the previous section and is consistent with the upper bound of 0.07 provided by Petrich and Eicken (2017). The observation that the critical porosity appears to govern the bulk salinity of congelation ice even at low temperature gradients ($\sim 10^{-8}$) lends credence to its potential for governing the stable salinity of an ice shell formed through directional freezing.

4.2.2. Marine Ice

The distribution coefficients associated with marine ice can be lower than the equilibrium distribution coefficients for congelation ice by up to an order of magnitude (Table 2 and Fig. 4), generally falling between 10^{-4} and 10^{-3} (bulk salinities between 10^{-2} and 10^{-1} ppt). The salinity profiles associated with marine ice (Fig. 4b,c) generally appear to depict a decrease with distance from the meteoric-marine interface within the impermeable portion of the ice core and an increase from the permeable-impermeable boundary to the ice-ocean interface. Note that many of the profiles depicted in Fig. 4 do not extend to the permeable layer, so we must rely on descriptions of the drilling and isolated samples reported in the published works to infer its properties.

The salinity profiles of the Roi Baudouin Ice Shelf cores are anomalously high relative to those of other marine ice cores (Fig. 4b,c) and approach values comparable to that of sea ice. Recent consolidation was proposed as an explanation for the high salinity of the Roi Baudouin cores (Pattyn *et al.* 2012), implying that young marine ice may initially present with salinities commensurate with sea ice but will gradually desalinate and approach a steady state over time due to increased accumulation and consolidation. This interpretation is supported by their salinity profiles, which depict a stable salinity similar to that of the marine ice at McMurdo Ice Shelf that transitions to an increasing salinity with depth (Fig. 4c). An alternative explanation is that the Roi Baudouin marine ice formed in a high temperature gradient environment and is analogous to platelet ice. However, the site is not unlike the rift at Nansen Ice Shelf where the salinity of the marine ice there was found to be in-family with other marine samples (Khazendar *et al.* 2001; Tison *et al.* 2001). The rift at Nansen Ice Shelf is located in an area with strong katabatic winds, which could result in the ablation of the marine ice which originally infilled the rift (Khazendar *et al.* 2001). This suggests the marine ice exposed at the surface may have formed at a lower depth, much like at Hells Gate Ice Shelf where katabatic winds expose basal marine ice at the surface near the ice shelf terminus (Souchez *et al.* 1991). This suggests marine ice at Nansen ice shelf may have initially shared characteristics with that of Roi Baudouin but became more homogenous and consolidated over time.

The age of the marine ice appears to be a more dominant factor in governing the bulk salinity than the temperature gradient, supporting the idea that the consolidation mechanism is a compaction and not congelation process. This is evident from the plots in Fig. 4c which demonstrate that increased depth does not correlate to decreased salinity. Although the Dailey Island cores correspond to the lowest salinity marine ice samples (Fig. 4c), because $\delta^{18}O$ was not measured, the role of glacial meltwater in reducing the salinity cannot be discounted. The salinities of the Nansen Ice Shelf core, Filchner-Ronne Ice Shelf core, and the Amery Ice Shelf core are approximately equal although they were sampled from depths that differed by over 100 m from each other. The profiles associated with the Amery Ice Shelf and Nansen Ice Shelf cores suggest the salinity could continue decreasing beyond the region sampled. The Filchner-Ronne Ice Shelf core, on the other hand, shows evidence of achieving a stable salinity near the base of the core. We thus adopt $k_{eq} = 6.9 \times 10^{-4}$ as the effective equilibrium solute distribution coefficient for low temperature gradient frazil ice, which corresponds to the stable salinity of the

consolidated layer estimated using the salinity at the base of the Filchner-Ronne Ice Shelf core (Fig. 4).

5. **Accretion beneath the Ice Shells of Ocean Worlds**

Although there have been no direct observations of the interior of the ice shells of ocean worlds, features observed at the surfaces or inferred about the ice shell topography have led to the development of hypotheses for processes that either directly appeal to the accretion of ice at the ice-ocean interface or are consistent with conditions that promote it (e.g., Soderlund *et al.* 2020). These features are scars of processes which modify bulk ice shell properties and serve as a record of heterogeneities introduced into the native shell.

5.1. Bulk Salinity of a Congelation Ice Shell

We estimate the bulk salinity of the ice shell as the product of congelation ice growth at the ice-ocean interface using a 1D solidification model known as the Stefan problem, where heat is conducted from the interface through the overlying ice. The analytical solution to this problem represents the temperature in the ice, T, as a function of position, x, and time, t, and is given by

$$T(x,t) = T_s + (T_f - T_s)\frac{\mathrm{erf}\left(\frac{x}{2\sqrt{\alpha t}}\right)}{\mathrm{erf}(\lambda')} \quad (1)$$

where T_s is the surface temperature, T_f is the freezing temperature, α is the thermal diffusivity of the ice, and λ' is the solution to the equation

$$\lambda' e^{\lambda'^2}\,\mathrm{erf}(\lambda') = \frac{N_{Ste}}{\sqrt{\pi}} \quad (2)$$

where N_{Ste} is the Stefan Number, defined as

$$N_{Ste} = \frac{c_p(T_s - T_f)}{L} \quad (3)$$

where c_p is the specific heat capacity of ice and L is the latent heat of fusion. The position of the ice-water interface as a function of time can be expressed in terms of these variables as

$$X(t) = 2\lambda'\sqrt{\alpha t} \quad (4)$$

and the velocity of the ice-water interface is

$$\dot{X}(t) = \lambda'\sqrt{\frac{\alpha}{t}} \quad (5)$$

which corresponds to the time derivative of Eq. 4. We use Eq. 5 to estimate ice shell growth rate as a function of the ice-water interface position, represented by ice thickness (Fig. 5). We assume the ocean is at the melting temperature of 270 K and that the thermophysical properties of the ice shell are represented by pure ice at this same temperature at 1 atm (Feistel and Wagner 2006). We evaluate four cases, assuming upper boundary conditions of 50 K, 100 K, 200 K, and 250 K to approximate surface temperatures expected at icy ocean worlds. 50 K represents a lower bound surface temperature for both Europa and Enceladus, 100 K represents the mean annual surface temperature of Europa's ice shell (Ojakangas and Stevenson 1989; Ashkenazy 2019), 200 K represents the maximum temperature near the tiger stripes of Enceladus (Spencer *et al.* 2018), and 250 K is intended to represent a terrestrial boundary condition. Higher surface temperatures result in lower growth rates for a given ice shell thickness. Using this model, we can estimate an upper bound on ice shell growth rate and thus estimate the maximum salinity of the bulk ice shell.

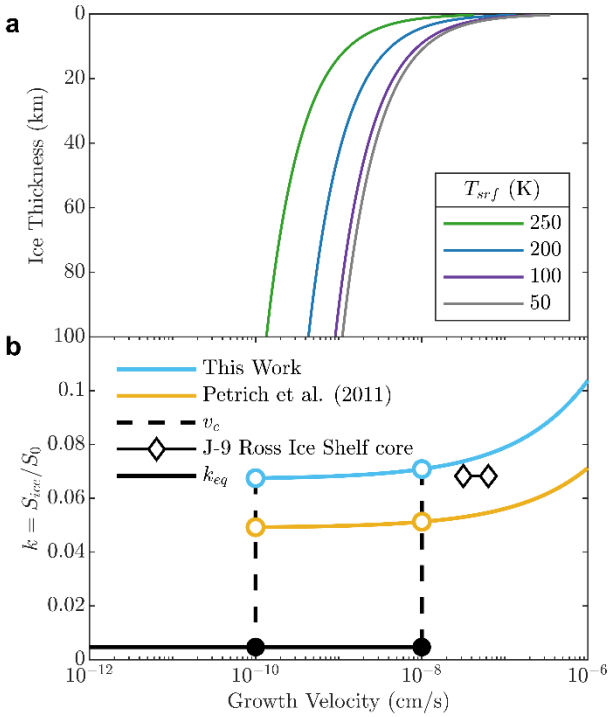

Figure 5. (a) Ice shell thickness vs. growth velocity and **(b)** effective solute distribution coefficient vs. of growth velocity. The effective solute distribution coefficient curves are taken from Fig. 3. The dashed line represents an illustration of the transition from a cellular interface to a planar interface at a critical growth velocity, v_c, represented by two possible values. The solid line depicts the equilibrium solute distribution coefficient. The diamond markers represent the bounds of growth velocity estimated by Zotikov *et al.* (1980) for the J-9 Ross Ice Shelf core.

Instead of explicitly modeling salt rejection, like Buffo *et al.* (2020) and Buffo *et al.* (2021), we represent the incorporation of salt as a function of growth velocity using a model for $k(v)$, adapted from Petrich *et al.* (2011). We prescribe a critical porosity equal to the effective equilibrium distribution coefficient for congelation ice $\phi_c = k_{eq}$, as opposed to $\phi_c = 0.05$ which

is used in the model of Petrich *et al.* (2011), and force the model to approach this value at low growth velocities. This yields an expression for the effective solute distribution coefficient given by

$$k(v) = k_{eq}\left(1 + \frac{k_{eq}}{2}\frac{v}{\gamma_s w_0}\left[-1 + \sqrt{1 + \frac{4(1-k_{eq})}{{k_{eq}}^2}\frac{\gamma_s w_0}{v}}\right]\right) \quad (6)$$

where k_{eq} represents the effective equilibrium solute distribution coefficient for congelation ice, v is the ice growth velocity, and $\gamma_s w_0$ represents a scaling parameter related to the interstitial brine velocity (Petrich and Eicken 2017). Note that our version includes an additional factor of 2 that was excluded from a term in the radicand in the published versions of the original model (Petrich *et al.* 2011; Petrich and Eicken 2017). We fit Eq. 6 to the data of Nakawo and Sinha (1981) to obtain $\gamma_s w_0 = 3 \times 10^{-8}$ m/s which is similar to the value of $\gamma_s w_0 = 4.5 \times 10^{-8}$ m/s obtained by Petrich *et al.* (2011). Both our model and the original model are shown alongside the data of Nakawo and Sinha (1981) in Fig. 3. We estimate the bulk salinity of the ice shell using Eq. 6 and the growth velocities obtained from the 1D freezing model (Eq. 5). We find that the growth velocity transitions to the ice shelf regime (Fig. 3) below ~100 m depth for all surface temperatures considered. This is similar to the results of Buffo *et al.* (2020) which found the salinity profile approaches an asymptotic value below ~300 m. This supports the conclusion that the bulk salinity for a large fraction of the ice shell will correspond to a value approaching the effective equilibrium solute distribution coefficient. Note that the lower limit bulk ice shell salinity predicted by Buffo *et al.* (2020) corresponds to an effective equilibrium solute distribution coefficient governed by the apparent critical porosity in congelation ice (~0.05). We instead adopt an effective equilibrium solute distribution coefficient of $k_{eq} = 6.7 \times 10^{-2}$, derived from the Ross Ice Shelf core in Section 4.2.1 to represent the bulk salinity of a congelation ice shell.

Although the critical porosity appears to be a significant factor governing the effective equilibrium solute distribution coefficient in natural congelation ice, as the growth velocity approaches zero, the ice-water interface geometry should become planar and as a result will be incapable of entrapping brine (Eicken 1998). A planar interface is generally stable for lake ice on Earth because of the relative purity of the water ($\lesssim$ 1 ppt); however, the same phenomenon can occur if the growth velocity falls below a critical growth velocity for a higher salinity water (Wettlaufer 1992; Maus 2007). The development of a stable planar interface under the appropriate growth conditions is a phenomenon that has been studied in both nature and laboratory experiments for decades (Weeks and Lofgren 1967; Grothe *et al.* 2014). In experiments the transition from a cellular to planar interface coincides with a drastic change in appearance (cloudy to clear) and a reduction in effective solute distribution coefficient that can exceed an order of magnitude (Weeks and Lofgren 1967; Osterkamp and Weber 1970; Kvajić and Brajović 1971; Maus 2006). This suggests the potential existence of a congelation ice shell where the bulk salinity is not governed by the critical porosity.

Although the existence of a critical growth velocity is not controversial, the magnitude of the critical growth velocity for a solution of a given salinity is challenging to constrain. Morphological stability theory (MST), originally proposed by Mullins and Sekerka (1964), has

been leveraged by a number of authors to investigate the development of a cellular interface in the freezing of saltwater systems (Wettlaufer 1992; Maus 2007). The theory has been augmented through the years (Coriell *et al.* 1985; Sekerka *et al.* 2015) and is still an active area of research (Maus 2020). The theory predicts the existence of a critical growth velocity below which a planar ice-water interface should be stable for any wavelength perturbation. The magnitude of this critical growth velocity is poorly constrained by theory and is highly sensitive to parameters including the solution concentration (i.e., salinity), the interfacial solute distribution coefficient (S_{ice}/S_{int}), and the temperature gradient in the liquid (Terwilliger and Dizio 1970; Wettlaufer 1992; Maus 2006; Maus 2020). To illustrate the onset of this transition during the thickening of an ice shell (Fig. 5), we adopt the values obtained by Wettlaufer (1992) from a linear stability analysis applied to the interface morphology of a sodium chloride system for a solution concentration approximately equal to Earth's ocean (~35 ppt). The critical growth velocity of $v_c \approx 10^{-8}$ cm/s assumes an interfacial solute distribution coefficient of 0.3, whereas $v_c \approx 10^{-10}$ cm/s assumes an interfacial solute distribution coefficient of 0.003. Their results demonstrate that the more efficient the ice is at rejecting the solute, the lower the critical velocity for the onset of interface instability for a given solution concentration. The upper estimate for critical growth velocity is reached for an ice shell thickness less than ~10 km for all surface temperatures considered (Fig. 5). Again, note that we adopt the values in Fig. 5 for illustration purposes only and the true value could be orders of magnitude lower.

Below the critical velocity, we assume a planar-ice water interface remains stable and that the bulk salinity of the ice shell will be governed by the equilibrium distribution coefficient (note the absence of "effective") for congelation ice, where impurities are retained predominantly within the ice lattice (i.e., not incorporated interstitially as brine). However, soluble salts can be accommodated in the ice lattice only up to a certain concentration referred to as the solubility limit. From both natural and artificial samples, the solubility limit for chloride in ice has been inferred to be $\sim 300\ \mu$M (Seidensticker 1972; Gross *et al.* 1977; Moore *et al.* 1994), although in the presence of ammonium the solubility limit increases (Gross *et al.* 1977). There is some evidence that the solubility limit may be higher in ice that has undergone recrystallization (Moore *et al.* 1994), suggesting marine ice may be able to accommodate more chloride than sub-ice shelf congelation ice. The chloride distribution coefficients obtained by Gross *et al.* (1977) represent salt entrainment through incorporation of impurities in the ice lattice and serve as the lower bound of equilibrium distribution coefficients for congelation ice. Their values are similar to earlier works that estimated equilibrium distribution coefficients on the order of 10^{-3} for dilute ($\sim 2 \times 10^{-4}$ M) chloride solutions (Osterkamp and Weber 1970). For solution concentrations where chloride could be entirely accommodated within the ice lattice ($\lesssim 10^{-1}$ M) and did not occupy interstitial sites, the average equilibrium distribution coefficient was determined to be $k_{eq} = 2.7 \times 10^{-3}$ (Gross *et al.* 1977). Note that this distribution coefficient applies to chloride and not the associated cation pair, which was found to be significantly less soluble (Gross *et al.* 1977). In the presence of ammonium, the equilibrium distribution coefficient increased to $k_{eq} = 1.4 \times 10^{-2}$ (Gross *et al.* 1977). For more concentrated solutions, the solubility limit was exceeded upon crystallization, forcing residual impurities to be accommodated interstitially along grain boundaries. In this case the distribution coefficient increased to $k_{eq} = 4.7 \times 10^{-3}$ (Gross *et al.* 1977; Tison *et al.* 2001). Although the distribution coefficient almost doubled at this transition, it was independent of the solution concentration

both below and above this transition. It is unclear whether a solution composed entirely of insoluble salts, such as magnesium sulfate, would be accommodated as efficiently because it would be limited to interstitial sites. It is also possible that because of its inability to be accommodated in the lattice, a solution dominant in lattice insoluble salts may promote interface breakdown and enhance interstitial entrapment.

These models imply that the native bulk salinity of a congelation ice shell should be <10% of the ocean salinity, where sub-ice-shelf congelation ice cores imply a bulk salinity between 6% and 7%. There are two cases where we might expect a higher salinity layer to be present near the ice shelf surface: (i) catastrophic melting and subsequent refreezing of an ice shell, although this would likely only extend to ~100 m depth, and (ii) rapid refreezing of intrusive features, if they extend far enough into the cold ice shell interior (Buffo *et al.* 2020). If the ice shell growth velocity is sufficiently slow, such that a planar interface remains stable as the ice shell thickens, the ice shell salinity reduces to <1% of the ocean salinity. For a planar interface at near-equilibrium conditions, the salts entrained are dominantly lattice soluble salts, such as chloride. The experiments of Gross *et al.* (1977) suggests the ice chlorinity will be 0.27% of the ocean chlorinity. In the case that the chlorides cannot be entirely accommodated within the lattice, the ice shell chlorinity will be 0.47% of the ocean chlorinity and permit some interstitial incorporation of impurities. Diagenetic processes can operate to alter the bulk ice shell salinity post-accretion. Flushing of interstitial impurities by meltwater could locally reduce the ice shell salinity, whereas refreezing of meltwater could locally enhance the ice shell salinity. In the ice shells of ocean worlds, meltwater may be generated through tidal heating (Sotin *et al.* 2002), through frictional heating caused by tectonic activity (Gaidos and Nimmo 2000; Nimmo and Gaidos 2002), or by convective currents (Kalousová *et al.* 2014). Whether this melt can drain through the ice shell is critically dependent on the ice shell permeability (Kalousová *et al.* 2014; Hesse *et al.* 2020). If interstitial impurities are removed due to flushing or drainage, the bulk salinity would be governed by concentration of impurities accommodated in the ice lattice. For ice saturated with chloride, this would imply an ice shell chlorinity of ~10 mg/kg which is on the order of ice shell salinity predicted by Steinbrügge *et al.* (2020).

Fluctuations in ice shell growth rates have the potential to generate vertical and regional heterogeneities in ice shell salinity. However, predicted growth rates suggest fluctuations are likely to fall within the low growth velocity regime (Table 2, Figure 3), where the effective solute distribution coefficient is relatively insensitive to changes in growth velocity. Peddinti and McNamara (2019) predict an increase in growth rate from 5.67 km/Myr to 8.22 km/Myr associated with the merging of convective cells within Europa's ice shell, which translates to growth velocities of 1.8×10^{-8} to 2.6×10^{-8} cm/s. Growth rate estimates obtained by other authors are typically on the order of 10^{-9} or 10^{-8} cm/s (Table 2). Comparing the lowest estimate of freezing rate for Europa's ice shell in Table 2 (~1.5 km/Myr) to the age of the surface (~100 Ma) would imply an ice shell thickness of ~150 km (Bierhaus *et al.* 2009). Because Europa's ice shell thickness is thought be an order of magnitude thinner, this suggests (i) the ice shell has reached a near-equilibrium thickness, (ii) the ice shell is in a state of thermodynamic disequilibrium where melting and re-freezing are occurring continuously, as suggested by Green

et al. (2021), or (iii) the estimated freezing rates are potentially an order of magnitude higher than reality. At Enceladus, observed topographic anomalies are thought to be maintained by melting/freezing less than a few mm/yr (Čadek *et al.* 2019; Kang *et al.* 2021), which translates to growth velocities on the order of 10^{-9} cm/s. These growth velocities are comparable to the upper estimate for critical growth velocity at which an ice-water interface becomes planar for a terrestrial ocean (Wettlaufer 1992). If transitions in growth velocity are such that the ice-water interface stability is affected, this could result in a salinity contrast of up to an order of magnitude associated with this event (Fig. 5). A similar magnitude salinity contrast could be generated by the local and regional accretion of marine ice beneath congelation ice.

5.2. Local and Regional Accretion of Frazil Ice

The ice-ocean interfaces of icy ocean worlds represent dynamic environments characterized by gradients in ice thickness on both regional and local scales (Nimmo *et al.* 2007; Nimmo and Bills 2010; Čadek *et al.* 2019; Hemingway and Mittal 2019; Soderlund *et al.* 2020).

Rifts and basal features, such as crevasses and troughs, represent favorable locations for the formation and accretion of frazil ice in an ice shell. A number of processes have been demonstrated to generate stresses sufficient to cause fracturing in the ice shell including impacts (Craft and Roberts ; Turtle and Pierazzo 2001), pressurization due to cooling and thickening (Nimmo 2004b; Manga and Wang 2007; Johnston and Montési 2017; Hemingway *et al.* 2020), tidal forcing/nonsynchronous rotation (Helfenstein and Parmentier 1985; Geissler *et al.* 1998; Greenberg *et al.* 1998; Hoppa 1999; Lee *et al.* 2005; Hurford *et al.* 2007; Rhoden *et al.* 2012; Patthoff *et al.* 2019), and true polar wander (Schenk *et al.* 2008; Rhoden *et al.* 2011; Tajeddine *et al.* 2017).

The fracturing of an ice shell has important implications for surface-ice-ocean exchange and as such has been studied extensively. Early work by Crawford and Stevenson (1988) examined both surface and basal fractures as resurfacing mechanisms for Europa's ice shell. They found that direct conduits extending from the surface through an ice shell were unlikely due to the need for high stresses applied rapidly which cannot be supplied by any process thought to be operating at Europa. Basal fractures were also shown to be incapable of extending to the surface; however, they extended over an order of magnitude farther than surface fractures. Although basal ice is ductile, Crawford and Stevenson (1988) argue that crack initiation and propagation is possible if the ice is strained sufficiently rapidly compared to the Maxwell time. This condition is possibly satisfied by the eccentricity tides which are ~10^5 s and comparable to the Maxwell time of ~10^4 s (Crawford and Stevenson 1988). The model of Lee *et al.* (2005) showed that surface fractures could penetrate the entire brittle part of the ice shell, in the case where a brittle and ductile layer are mechanically decoupled. They did not study basal fractures, citing that they were less likely to occur than surface fractures based on the increase in ice strength with depth, due to pore closure, and their interpretation of the results of Crawford and Stevenson (1988). Rudolph and Manga (2009) show that in the presence of a relaxed basal layer, fractures on Europa cannot penetrate the ice shell for thicknesses greater than a few kilometers. Because the gravitational acceleration at Enceladus is a fraction of that at Europa, fractures could penetrate the ice shell for

thicknesses up to tens of kilometers (Rudolph and Manga 2009). The ice shell thickness where the tiger stripes are located is thought to be less than 10 km (Hemingway *et al.* 2020), supporting the interpretation that these features are fractures connecting the ice shell surface to a subsurface ocean (Postberg *et al.* 2011; Spencer *et al.* 2018). The ice collapse model of Walker and Schmidt (2015) suggests basal fractures could form above a subsurface water pocket; however, this mechanism would not necessarily translate to the formation of basal fractures at an ice-ocean interface. Hemingway *et al.* (2020) argue that a surface fracture could penetrate a ductile ice layer in an ice shell, so long as it is not too thick, because the layer will behave elasticity on timescales relevant to fracture propagation. Walker *et al.* (2021) show that tensile fractures initiating from the base of an ice shell can propagate further into the interior than surface fractures. Furthermore, they showed that connection between the surface and ice-ocean interface can be achieved if basal tensile fractures connect to the surface through shear failure.

Broadly these works suggest basal fractures extending into the ice shell interior are possible—if the basal ice is subject to a sufficiently high strain rate—and that rifts extending through the entirety of an ice shell are unlikely for Europa but possible under specific conditions. Still, many authors attribute surface features at Europa such as domes, pits, and lenticulae to the presence of sills within the ice shell and implicate vertical fractures extending from the ice-ocean interface in their formation (e.g., Michaut and Manga 2014; Craft *et al.* 2016). Furthermore, observations and interpretations of putative plume activity at Europa (e.g., Sparks *et al.* 2017; Jia *et al.* 2018) and Enceladus (e.g., Postberg *et al.* 2011) provide strong evidence that fractures in the ice shell serve as a connection between the surface and some subsurface water reservoir. Where cracks may penetrate the entirety of an ice shell, such as the tiger stripes at Enceladus, the resulting plumes would likely include samples of relatively unfractionated ice formed from agglomerated frazil crystals that nucleated within the turbulent, supercooled water column as the ocean water was brought to the surface. Given the fast rate of ice formation, the salinity and compositional signal likely experiences minimal fractionation, $k \approx 1$. Conversely, if the plume material were sourced from a reservoir generated from the melt of native ice shell material and not the ocean, our estimate of the effective equilibrium solute distribution coefficient for a congelation ice shell ($k_{eq} = 6.7 \times 10^{-2}$) would predict a saturated ocean at Enceladus (20 ppt/0.067 ~ 300 ppt). This estimate neglects the effect of brine concentration that may occur during freezing of a reservoir. At Enceladus, plume material is thought to be sourced directly from a sub-ice ocean (Spencer *et al.* 2018); however, the origin of plumes at Europa is more ambiguous (Sparks *et al.* 2017).

Ice shell thickness variations on regional scales have been inferred from models and observations of ocean worlds. Models of the ice shell thickness of Enceladus based on observations of the shape (Tajeddine *et al.* 2017) and gravity (Iess *et al.* 2014) by *Cassini* suggest the presence of lateral variations in the ice shell thickness (Čadek *et al.* 2019). Limb profiles of Europa suggest either a thin ice shell (<35 km) with lateral thickness variations below the detection threshold or a thicker shell in which lateral flow or convection promote a uniform ice shell thickness (Nimmo *et al.* 2007). Although the ice shell thickness of Europa is more poorly constrained than Enceladus (Billings and Kattenhorn 2005; Howell 2021), multiple models have demonstrated variations in surface temperature and basal heat flux could promote lateral thickness gradients (e.g., Soderlund *et al.* 2013; Ashkenazy *et al.* 2018; Čadek *et al.* 2019; Soderlund 2019). These lateral thickness gradients could plausibly occur in any icy ocean world with large surface temperature gradients in latitude and/or heterogeneous tidal heating. Because these lateral

thickness gradients are unstable (both from a mechanical and thermodynamic perspective), mechanisms will operate to homogenize the ice shell thickness.

Two mechanisms have been proposed for the homogenization of ice shell thickness: (i) the pressure gradient induced by the variable ice thickness will drive basal ice flow from thicker to thinner regions of the ice shell (e.g., Ojakangas and Stevenson 1989; Nimmo 2004a; Nimmo *et al.* 2007; Ashkenazy *et al.* 2018) and (ii) an "ice pump", described by Lewis and Perkin (1986), will operate to melt ice where the ice shell is thick and accrete ice where the ice shell is thin (e.g., Vance and Goodman 2009; Soderlund *et al.* 2013). Both properties likely play a role in homogenizing ice shell thickness gradients, although environmental factors such as ocean circulation and tidal velocity will determine which process dominates (Goodman 2018). The ice flux resulting from viscous flow at the base of the ice shell has been estimated to range from fractions of a millimeter to centimeters per year at Europa (Ashkenazy *et al.* 2018) and less than a few millimeters per year at Enceladus (i.e., on the same timescales as melting) (Kamata and Nimmo 2017), whereas marine ice accretion rates on Earth, driven by the "ice pump" are on the order of meters per year (Craven *et al.* 2009). We thus focus our discussion on the "ice pump" which could infill these features on shorter timescales than viscous flow. As the buoyant meltwater is transported along the ice-ocean interface in the direction of decreasing ice thickness, it will become supercooled due to the reduction in pressure and prime the generation of frazil ice.

For terrestrial ice shelves, the ice pump process is approximately adiabatic (Foldvik and Kvinge ; Tison *et al.* 1998; Koch *et al.* 2015; Hoppmann *et al.* 2020). Neglecting heat transfer between water masses is likely only a valid assumption over certain temporal and spatial scales, which may be exceeded when applied to regional scale thickness gradients in the ice shells of ocean worlds. Crevasses, troughs, and rifts, on the other hand, represent high gradient features that can promote substantial supercooling through the operation of a highly localized ice pump. The magnitude of potential supercooling will be governed by the feature's vertical extent in the ice shell, equivalent to the difference in the pressure melting temperature expected by a reduction in overburden pressure (Fig. 1). These high gradient features also provide a means to shelter the frazil from potentially strong sub-ice currents (Soderlund *et al.* 2020), allowing crystals to accumulate and consolidate, forming marine ice. This process is analogous to the infilling of rifts at the Nansen and Roi Baudouin Ice Shelves by marine ice (Fig. 4). The texture of the Nansen Ice Shelf core was not columnar, suggesting no congelation growth had occurred within the rift (Khazendar *et al.* 2001). This suggests the infilling of high gradient features in the ice shells of ocean worlds would likely be dominated by frazil ice, as opposed to congelation ice, by nature of both the localized ice pump and the relatively low temperature gradients expected near the base of the ice shell. In this case, the salinity profile will likely decrease with depth within the consolidated layer. At the permeable-impermeable boundary, the salinity may appear to level off before increasing again as the brine volume fraction increases with depth (Fig. 4). It is possible that if the fracture penetrated far enough into the ice shell such that the surrounding ice was substantially colder, congelation ice could play more of a role as modeled in Buffo *et al.* (2020).

6. **Implications of Accretion at the Ice-Ocean Interface**

6.1. Geophysical Implications of Heterogeneous Accretion

The accretion of frazil ice within basal features in a congelation ice shell has significant implications for processes governing surface-ice-ocean exchange. Frazil ice accretion serves as a vehicle to deliver both sensible heat and latent heat into the ice shell interior. Sensible heat is delivered through the introduction of warm ice (relative to the ice shell interior), as frazil infills and consolidates within basal features. The relative warmth of marine ice within an ice shelf is supported by borehole measurements from Amery Ice Shelf which show that the temperature profile within the marine ice layer is nearly isothermal at a temperature close to the freezing point of the underlying seawater (Craven *et al.* 2009). The gradual consolidation and interstitial freezing of brine pockets further releases latent heat into the ice shell, serving as an additional mechanism to thermally perturb the ice shell. Because of the timescales of tidal cycles on Enceladus, it is unlikely a highly-consolidated marine ice would be able to form within the tiger stripes; however, the formation and accumulation of frazil in the fissures could be capable of modulating eruptions, a role previously attributed to turbulent dissipation alone (Kite and Rubin 2016).

Marine ice is more ductile than meteoric ice (Holland *et al.* 2009; Jansen *et al.* 2013; Kulessa *et al.* 2014; McGrath *et al.* 2014); however, it is still an open area of research whether this could be an intrinsic material property or can be attributed to elevated temperatures alone (Dierckx and Tison 2013; Craw 2020). The infilling of basal features by more ductile ice could affect the mechanical properties of the ice shell. On Earth, marine ice accretion is thought to play an important role in stabilizing ice shelves against collapse through the infilling of regions of weakness (Holland *et al.* 2009; Khazendar *et al.* 2009; Kulessa *et al.* 2014) and could play a similar role in ice shells. The observation that fractures propagating in ice shelves arrest when encountering features infilled with marine ice (McGrath *et al.* 2014) could guide inferences of subsurface properties of an ice shell using observations of the fractured surface terrain. The accretion of marine ice within suture zones has been shown to channel shear deformation enabling decoupling of adjacent units of ice flowing at different velocities (Jansen *et al.* 2013). As such, accretion in pre-existing fractures could facilitate strike-slip and lateral displacement, thought to be responsible for the linea observed on Europa's surface (Hoppa 1999; Hoppa *et al.* 2000; Prockter *et al.* 2000; Hammond 2020). Enhanced ductility within these features might also favor heating over fracturing when subject to tidal deformation, potentially resulting in positive feedback. The enhanced ductility would also increase the Rayleigh number (ratio of buoyancy to diffusion), influencing convective vigor and modulating its responses to tidal forcing. This suggests marine ice accretion could also play a role in transitioning between convective and conductive regimes in an ice shell.

The marine ice infilling these features is not only warmer but could also be significantly purer than the native ice shell material (see Table 3). As such marine ice is both thermally and compositionally buoyant, which could further promote the formation of narrow diapirs thought to be responsible for forming Europa's domes (Pappalardo and Barr 2004). Soderlund *et al.* (2013) proposed that marine ice accretion on regional scales, modulated by thickness gradients

established by heterogeneous ocean-driven heating, could play a role in the formation of chaos terrain through a similar mechanism (Schmidt *et al.* 2011).

6.2. Fractionation

To constrain the habitability of an ocean worlds, it is important to determine whether the composition of the ice shell is representative of the underlying ocean. The mode of salt entrainment, whether salt is accommodated within the ice lattice or interstitially as brine pockets, can influence the ice shell composition. A cellular interface would be more favorable for the entrapment of brine pockets than a planar interface, resulting in a bulk ice composition more representative of the underlying ocean in terms of the *relative* concentrations of major ionic species. Because there are very few studies of the chemistry of low temperature gradient ice, we include studies of sea ice to identify processes that can result in fractionation of an ice shell.

The composition of sea ice is generally assumed to be representative of seawater (Petrich and Eicken 2017), although published studies of accreted ice chemistry suggest that some chemical fractionation occurs in sea and marine ice (Table 4). There does not appear to be any evidence that sulfate or calcium are consistently either enriched or depleted in sea ice, although potassium appears to be depleted across all sea ice samples presented in Table 4. This is consistent with the idea that the degree of fractionation should scale with ion diffusivity (Maus *et al.* 2011) because potassium represents the fastest diffusing ion and thus is more efficiently removed from the ice through networks of brine channels. The consistent enrichment of magnesium observed in sea ice (Table 4), cannot be attributed to known cryohydrate precipitation and is likely related to its slow diffusivity relative to chloride (Granskog *et al.* 2004; Maus *et al.* 2011). Although calcium and sulfate are also slow diffusing relative to chloride, these ions participate in cryohydrate formation early-on in sea ice growth ($T > -8$ °C) which could further influence the fractionation signal. Studies of fractionation in multi-year sea ice cores (Anderson and Jones 1985; Gjessing *et al.* 1993) and changes in fractionation with depth observed in young sea ice cores (Maus *et al.* 2011) suggest that the fractionation signal may evolve as the ice thickens and ages. The mixing model of Reeburgh and Springer-Young (1983) suggests that melt produced from warming as the ice ages removes ionic species conservatively; however, the sea ice samples of Gjessing *et al.* (1993) show strong sulfate depletion due to washout from melting snow. The enrichment observed in certain low salinity samples was interpreted to the result of refreezing of meltwater (Gjessing *et al.* 1993). Although mirabilite precipitation is often implicated in observed sulfate enrichment (Granskog *et al.* 2004), the results of Gjessing *et al.* (1993) and Maus *et al.* (2011) suggest sulfate enrichment could be due to the relatively low diffusivity of sulfate. Because chloride can be accommodated in the lattice, it can be preserved in the ice as other insoluble ions retained in interstitial brine are rejected (Moore *et al.* 1994). This phenomenon can be observed in samples of marine ice, where the degree of fractionation appears to increase and chloride becomes more enriched as brine volume fraction and salinity decreases (Moore *et al.* 1994). Snow ice similarly appears to retain chloride relative to other ions when flushed by meltwater, through a process termed preferential elution (Brimblecombe *et al.* 1987; Davies *et al.* 1987). Some studies have shown that sodium is removed at a similar rate to chloride and is the least mobile cation (Brimblecombe *et al.* 1985; Tsiouris *et al.* 1985; Brimblecombe *et al.* 1987; Davies *et al.* 1987),

967 which was been attributed to the role of sea salt in atmospheric condensation by Tsiouris *et al.*
968 (1985) but could also be related to adsorption effects (Davies *et al.* 1987). These early works
969 were validated by a recent study which was able to quantify the ion exclusion rates governing the
970 process of preferential elution (Costa *et al.* 2020).

971 **Table 4.** Fractionation reported in samples of sea ice and marine ice. Enrichment (+) and
972 depletion (–) is taken in reference to what is observed in seawater. Where the fractionation is
973 described as equal (=), the relative composition is considered to be within the uncertainty of
974 seawater. Where the fractionation is described as (+/–), some ice cores analyzed in the study
975 were enriched whereas others were depleted depending on sampling location. Where the
976 fractionation is described as (=/–), the samples broadly suggested relative depletion, but the
977 signal was not consistent across all depths. The fractionation presented for Maus *et al.* (2011)
978 corresponds to that of the bulk ice. The marine ice sample in Warren *et al.* (1993) corresponds to
979 the basal ice from Amery Ice Shelf. Ice type follows the same coding described in Fig. 4 (CS:
980 Congelation Sea Ice, M: Marine Ice).

Ice Type	Ca/Cl	K/Cl	SO_4/Cl	Na/Cl	Mg/Cl	Source
CS	–	–	+	=	+	Addison (1977)
CS	N/A	N/A	+/–	N/A	N/A	Reeburgh and Springer-Young (1983)
CS	–	N/A	+/–	N/A	N/A	Anderson and Jones (1985)
CS	=	–	=	=	+	Meese (1989)
CS	=	N/A	–	=	=	Gjessing *et al.* (1993)
CS	+	–	+	=	+	Granskog *et al.* (2004)
CS	=	–	–	+	–	Maus *et al.* (2011)
M	=	+	–	=	–	Warren *et al.* (1993)
M	=/–	=/–	–	–	–	Moore *et al.* (1994)
M	N/A	N/A	N/A	N/A	–	Koch *et al.* (2015)

981

982 These studies of terrestrial ice fractionation allow us to identify the processes that may alter the
983 chemical fingerprint of the sub-ice oceans of Europa and Enceladus in their ice shells:
984 differential diffusion and flushing by meltwater. An ice shell that entrains salt through the
985 entrapment of brine pockets should initially be representative of the underlying ocean. This is
986 also true for locations where frazil ice accretion occurs, although there will be some chloride
987 enrichment that will decrease with depth, inversely correlated to salinity and brine volume
988 fraction. If permeable brine networks remain stable over geologic time, differential diffusion
989 may result in a relative enrichment in magnesium and depletion in potassium. This diffusion can
990 still occur through the ice crystals in the absence of brine networks, although far less efficiently
991 (Price 2000). The presence of magnesium in the ice shell supports the hypothesis put forth by
992 Brown and Hand (2013) that magnesium salts from the ocean contribute to the radiolytic
993 formation of magnesium sulfate salts at the surface of Europa. The presence of sulfate salts at
994 surface of the ice shell is not necessarily incompatible with their early precipitation. If the ice
995 becomes impermeable at a temperature above which any cryohydrates precipitate, then the
996 composition of the ice should not differ significantly from that of the sub-ice ocean. If
997 cryohydrates were to precipitate in a permeable medium, there is the potential that flushing from
998 melt could remove these impurities from the ice, assuming brine veins were large enough to

transport the minerals. In the case where a planar microstructural ice-water interface remains stable at very low growth velocities, only impurities which are soluble in the ice lattice, such as chloride, would be incorporated in the ice shell. A similar mechanism to generate an ice shell dominated by chloride is by continuous flushing of interstitial impurities by meltwater. In the case where all brine is drained from the ice shell, chloride could still be preserved within the ice lattice. This indicates that although chloride salts have been observed on the surface and are correlated with endogenous features (Trumbo *et al.* 2019), this does not necessarily imply that the ocean is dominantly composed of chloride salts. Furthermore, the association of chloride with resurfacing features is compatible with the near-surface injection of a chloride-rich brine, where sulfate minerals remain in the subsurface, consistent with the hypothesis of Schmidt *et al.* (2011) for chaos terrain formation and evolution. Vance *et al.* (2019) also suggest that an ocean rich in sulfates may not be reflected in Europa's surface composition and attribute this to fractional crystallization (i.e., sulfate minerals precipitate out of solution earlier than chloride minerals).The drainage and subsequent refreezing of melt will likely play an important role in redistributing sulfate in the ice shell, generating regions of local sulfate depletion and enrichment, respectively (Gjessing *et al.* 1993; Maus *et al.* 2011).

6.3. Astrobiological Implications

Constraining the detailed physical structure and chemical characteristics of planetary ices has important implications for potential ice-ocean habitats and their ability to retain biosignatures. In icy world systems (e.g., Europa, Enceladus), the stratigraphic and structural evolution of the ice shell, including porosity, temperature, and chemistry, will determine the spatial habitability of the respective cryosphere and determine the preservation/degradation of biosignatures as they are transported through the ice shell (Schmidt 2020). Water activity (the availability of water) is an important metric which strongly influence the ability of organisms to persist in extreme environments (Oren 2008; Tosca *et al.* 2008).

Liquid vein networks and brine pockets are important habitats in both sea ice and glacial ice on Earth (Price 2000; Price 2007; Price 2009). Although the brine channels that form in sea ice are recognized as a significant cryosphere habitat (Loose *et al.* 2011; Arrigo 2014), the ice must maintain sufficient permeability to enable nutrient exchange in support of maintaining these habitats. For this reason the cool, impermeable sea ice interior is considered to be a less favorable environment for organisms relative to the ice-water interface, even though the interior represents an environment where sunlight is more accessible (Arrigo 2014). Beneath glacier ice, nutrient exchange within liquid vein networks is considered important to maintaining in-ice habitats in the absence of sunlight (Price 2000; Price 2007; Price 2009). Even so, the discovery of sub-ice-shelf anemones which burrow into relatively impermeable glacial ice suggests that organisms may not be inhibited by the lack available pathways through the ice (Daly *et al.* 2013). The complex relationship between ice permeability and habitability is highlighted by studies of sea ice microorganisms that generate extracellular polysaccharide substances (EPS) (Krembs *et al.* 2011; Raymond 2011). Although the brine volume fraction in ice is increased in the presence

of EPS, the similarly enhanced tortuosity results in a net decrease in permeability which allows brine to be retained in the ice (Ewert and Deming 2013).

The ability for ice to entrain biosignatures can also be examined independently from its suitability as a habitat. Studies of sea ice have shown that frazil ice can concentrate biological material through mechanical incorporation resulting from the buoyant consolidation of frazil ice crystals (Garrison *et al.* 1983; Clarke and Ackley 1984; Garrison *et al.* 1989). Frazil ice also possesses the unique ability to scavenge material as it is transported through a water column (Garrison *et al.* 1989; Reimnitz *et al.* 1993; Arrigo *et al.* 2010). A notable example of these scavenging capabilities can be observed in McMurdo Sound, where benthic fauna, mobilized by anchor ice (i.e., frazil that accretes at the seabed), have been found at the surface of the ice shelf (see Mager *et al.* 2013). There have not been many dedicated studies examining the incorporation of biosignatures in marine ice; however, one study of protists in the marine ice of Amery Ice Shelf revealed that these organisms were likely sourced from melting sea ice in the neighboring bay and were entrained in the ice as the meltwater was transported beneath the ice shelf (Roberts *et al.* 2006). This is significant because although marine ice did not serve as the original habitat to these organisms, it could incorporate and preserve these life forms even in the uppermost portion of the ice.

On ocean worlds, radiolytically generated oxidants transported from the surface may represent a viable alternative to sunlight for sub-ice organisms (Chyba 2000). If oxidant-limited, organisms within the sub-ice ocean will preferentially inhabit the ice-ocean interface where the ice shell serves as source of oxidants. Vertical motion of the ice-water interface driven by tidal deflection of the ice shell could promote nutrient exchange by permitting an influx of ocean water into the ice interior that might replenish habitats at the ice-ocean interface, similar to the tidally-driven recharge of nutrients in sea ice (Arrigo *et al.* 1995; Arrigo and Thomas 2004). The enhanced permeability of frazil ice relative to congelation ice may translate to more efficient tidally-driven nutrient exchange at interfaces dominated by such an ice texture and thus perhaps a more favorable habitat. An impermeable ice shell interior may imply a reduced concentration of preserved biosignatures if organisms migrate with brine towards the ice-ocean interface. Alternatively, the presence of EPS might prevent the drainage of brine habitats, through altering the structure of the ice, and preserve biosignatures even as the habitat becomes progressively more depleted in nutrients over time. Even if the ice-ocean interface is not inhabited, if life is present in the source water where frazil ice forms, biosignatures will likely be entrained as the frazil rises buoyantly to accumulate and consolidate at the ice-ocean interface. Because the relatively pure frazil ice is also buoyant relative to the surrounding ice shell, it can serve as a vehicle to deliver samples towards the surface where they might be sampled by a lander. Features associated with conditions favorable to the accretion of frazil ice can thus serve as promising sites for in situ investigations searching for signs of life.

An additional constraint on biological viability as well as biosignature preservation is the chaotropicity and kosmostropicity of fluids within the shell. A measure of the tendency for solutes to stabilize (kosmotropes) or destabilize (chaotropes) proteins and membranes, chao-/kosmo-tropicity impacts the habitability of brines and could limit the survivability of detectable biosignatures as they are transported through the ice shell and subjected to thermal cycling

(Hallsworth *et al.* 2007; Oren 2013; Pontefract *et al.* 2017). In many naturally occurring, charge balanced systems, the presence of kosmostropes offsets the destabilizing nature of chaotropes (e.g., seawater); however, if ions are preferentially fractionated through freezing or precipitation reactions, this balance can be upset and lead to toxic chaotropic solutions (Pontefract *et al.* 2017; Brown *et al.* 2020). One notable chaotrope is chloride, suggesting that an amplified presence in an ice shell due to fractionation could challenge resident biology if concentrations are high enough (Fox-Powell *et al.* 2016). The ice salinity and fractionation thus play an important role in determining the contemporary habitability of the ice shell as well as controlling the preservation of relict biosignatures. As such, constraining the ice-ocean interface dynamics—which govern the solute entrainment within and biogeochemical evolution of the shell—is an imperative part of assessing the habitability of ice-ocean worlds and designing life detection missions (Des Marais *et al.* 2008; Council 2011; Hendrix *et al.* 2019)

7. **Conclusions**

We have demonstrated that conditions at the ice-ocean interfaces of Europa and Enceladus (e.g., composition, temperature, and pressure) could be similar to those found on Earth. We show that ice which forms in the low temperature gradient environment beneath ice shelves in Antarctica could represent a more relevant analog than sea ice. Through a systematic review of published ice core samples collected in this low temperature gradient regime, we argue that the critical factors governing the bulk salinity of ice at the low growth velocity conditions expected at the ice-ocean interfaces of icy ocean worlds are the mechanism of accreted ice formation (frazil vs. congelation) and the microstructural interface geometry (planar vs. cellular). Figure 6 summarizes scenarios compatible with the formation of frazil and congelation ice beneath the ice shells of ocean worlds. Estimates of the bulk salinity associated with each mechanism are shown, expressed in terms of an effective equilibrium solute distribution coefficient, which is defined as the ratio of the bulk ice salinity to the salinity of the source water as the growth velocity approaches zero.

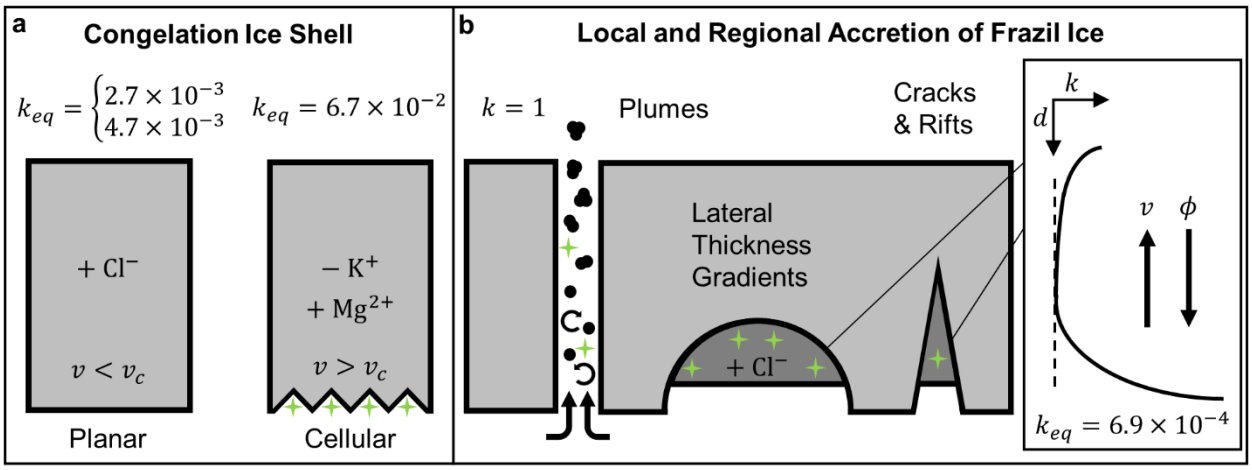

Figure 6. Sketch depicting bulk properties of **(a)** a congelation ice shell which formed in the growth velocity regime where $k \approx k_{eq}$, **(b)** frazil ice accreting in local and regional features, and **(c)** a profile of depth vs. solute distribution coefficient inspired by the salinity profiles of marine ice presented in Fig. 4. v represents the growth velocity of the ice, v_c is the critical growth velocity at which a planar ice water interface becomes unstable, k is the effective solute distribution coefficient, d refers to the depth from the accretion interface, and ϕ is the melt fraction of the ice. The $+/-$ in (a) depicts enrichment and depletion of impurities in the ice, respectively. The plume represented in (b) shows the nucleation of frazil in the turbulent water column as it as ascends and agglomerates. The green stars represent possible locations of biosignatures.

Cooling of the ocean will promote directional freezing and the formation of a congelation ice shell. Samples of sub-ice-shelf-congelation ice allow us to estimate the bulk salinity of an ice shell formed through congelation growth to be ~1% to ~10% of the ocean salinity. The upper bound effective equilibrium solute distribution coefficient derived from sub-ice-shelf congelation ice cores, $k_{eq} = 6.7 \times 10^{-2}$, incorporates salt by the entrapment of brine pockets, which would occur if the interface retained a cellular microstructure. The lower bound effective solute distribution coefficient, $k_{eq} = 2.7 \times 10^{-3}$, is derived from experiments and reflects growth conditions where a planar ice-ocean interface is stable. As such, this estimate only applies to salts that are soluble within the ice lattice, specifically chloride. If the chlorinity of the ice exceeds the lattice solubility limit for the lower bound distribution coefficient, any residual chlorides will be accommodated along grain boundaries and the lower bound distribution coefficient will increase to $k_{eq} = 4.7 \times 10^{-3}$. If fluctuations in ice shell growth rate occur that allow for transitions in interface morphology, the bulk ice shell salinity could change by an order of magnitude. The bulk salinity of frazil ice, which accumulates and consolidates in ice shell rifts and basal features, is estimated to be ~0.1% of the ocean salinity using an effective equilibrium solute distribution coefficient of $k_{eq} = 6.7 \times 10^{-4}$ derived from samples of marine ice.

Accretion at the ice ocean interface can influence ice shell geophysical processes, composition, the distribution of habitats and biosignatures, and dielectric properties. The infilling of ice shell crevasses and troughs by frazil can serve as a mechanism for introducing thermocompositional heterogeneities into the ice shell which could promote diapirism, influence convection, and

locally enhance tidal dissipation. Studies of fractionation in sea ice suggest the composition of a congelation ice shell should be approximately representative of the ocean; however, over timescales relevant to the age of the ice shell, diffusion could redistribute impurities such that the ice shell fractionation scales with both age and the mobility of impurities, provided sufficient permeability and concentration gradients are maintained. This would imply a relative enrichment in magnesium and depletion in potassium. Frazil ice accreting within basal features will become progressively more enriched in chlorides as salinity and brine volume fraction decrease towards the upper end of the ice column. Sulfates will be locally depleted and enriched where melt drainage and refreezing within the ice shell occurs, respectively. Low salinity samples of marine ice and studies of preferential elution in snow melt suggest that if interstitial salts are preferentially removed, such as through flushing of meltwater generated by tidal heating or tectonic activity, the ice shell will be enhanced in chlorides. An ice shell which maintains a planar interface during freezing would also be enriched in chlorides, further supporting the idea that a chloride-dominated surface is not an unambiguous indicator of a chloride-dominated ocean. An enrichment of chlorides could challenge the habitability of brine and preservation of biosignatures within the ice shell. Locations where frazil ice forms serve as promising targets for sampling potential biosignatures entrained from the ocean given the efficient scavenging abilities of loose crystals, high permeability within the unconsolidated layer which can be recharged with oceanic material by tidal action, and the potential for thermocompositional buoyancy to deliver the material to the surface. Congelation ice may promote higher brine volume fractions relative to frazil ice at given temperature due to its higher salinity; however, if the ice is impermeable this may not translate to a sustainable habitat.

The accretion of ice at the ice-ocean interface will govern the entrainment of oceanic material in the ice shell and serves as the primary filter controlling fingerprints of the ocean observable at the surface, including salinity, the relative concentration of major ionic species, as well as biosignatures. Understanding the eutectic behavior of planetary ice shells, which is directly dependent on the ice shell's composition, will improve habitability estimates for ice-ocean worlds by constraining brine volume fraction estimates as well as predictions of interstitial brine chemistry and water activity. Studies of terrestrial accreted ice can support verification and validation of planned and future missions to icy ocean worlds and serve to constrain the parameter space and detection limits for in situ and remote instrument design. Future work should leverage natural samples of these ices for improved characterization of thermal, mechanical, and electrical properties in support of these missions.

Acknowledgements

N. S. W. was supported by the G. Unger Vetlesen Foundation and the Zonta International Amelia Earhart Fellowship. K. M. S. was supported by NASA grant NNX14AR28G. D. D. B. was supported by the G. Unger Vetlesen Foundation. This work benefited from correspondence with Austin Green, John C. Moore, Lisa Craw, Lynnae Quick, Natalie Robinson, Sean Hsu, Sönke Maus, and Yosef Ashkenazy. The authors declare that they have no known competing financial interests or personal relationships which have or could be perceived to have influenced the work reported in this paper.

References

Addison J. R. (1977) Impurity Concentrations In Sea Ice. *Journal of Glaciology*, 18: 117-127.

Anderson J., Schubert G., Jacobson R., Lau E., Moore W., and Sjogren W. (1998) Europa's differentiated internal structure: Inferences from four Galileo encounters. *Science*, 281: 2019-2022.

Anderson L. G., and Jones E. P. (1985) Measurements of total alkalinity, calcium, and sulfate in natural sea ice. *Journal of Geophysical Research: Oceans*, 90: 9194-9198.

Arrigo K. R. (2014) Sea ice ecosystems. *Annual Review of Marine Science*, 6: 439-467.

Arrigo K. R., Dieckmann G., Gosselin M., Robinson D. H., Fritsen C. H., and Sullivan C. W. (1995) High resolution study of the platelet ice ecosystem in McMurdo Sound, Antarctica: biomass, nutrient, and production profiles within a dense microalgal bloom. *Marine Ecology Progress Series*, 127: 255-268.

Arrigo K. R., Mock T., and Lizotte M. P. (2010) Primary producers and sea ice. *Sea ice*, 2: 283-325.

Arrigo K. R., and Thomas D. N. (2004) Large scale importance of sea ice biology in the Southern Ocean. *Antarctic Science*, 16: 471-486.

Ashkenazy Y. (2019) The surface temperature of Europa. *Heliyon*, 5: e01908.

Ashkenazy Y., Sayag R., and Tziperman E. (2018) Dynamics of the global meridional ice flow of Europa's icy shell. *Nature Astronomy*, 2: 43-49.

Bierhaus E. B., Zahnle K., Chapman C. R., Pappalardo R., McKinnon W., and Khurana K. (2009) Europa's crater distributions and surface ages. In: *Europa*, University of Arizona Press Tucson, pp 161.

Billings S. E., and Kattenhorn S. A. (2005) The great thickness debate: Ice shell thickness models for Europa and comparisons with estimates based on flexure at ridges. *Icarus*, 177: 397-412.

Brimblecombe P., Clegg S., Davies T., Shooter D., and Tranter M. (1987) Observations of the preferential loss of major ions from melting snow and laboratory ice. *Water Research*, 21: 1279-1286.

Brimblecombe P., Tranter M., Abrahams P., Blackwood I., Davies T., and Vincent C. (1985) Relocation and preferential elution of acidic solute through the snowpack of a small, remote, high-altitude Scottish catchment. *Annals of Glaciology*, 7: 141-147.

Brown E. K., Buffo J. J., Grantham M., Pontefract A., Glass J., Ingall E., Doran P., Toubes-Rodrigo M., Dion-Kirschner H., and Carr C. (2020) Trapped in the Ice: An Analysis of Brines in British Columbia's Hypersaline Lakes. *LPI*: 2218.

Brown M., and Hand K. (2013) Salts and radiation products on the surface of Europa. *The Astronomical Journal*, 145: 110.

Brown M. E. (2001) Potassium in Europa's Atmosphere. *Icarus*, 151: 190-195.

Buffo J., Meyer C., and Parkinson J. (2021) Dynamics of a Solidifying Icy Satellite Shell. *Journal of Geophysical Research: Planets*: e2020JE006741.

Buffo J., Schmidt B., and Huber C. (2018) Multiphase reactive transport and platelet ice accretion in the sea ice of McMurdo sound, Antarctica. *Journal of Geophysical Research: Oceans*, 123: 324-345.

Buffo J. J., Schmidt B. E., Huber C., and Walker C. C. (2020) Entrainment and Dynamics of Ocean-derived Impurities within Europa's Ice Shell. *Journal of Geophysical Research: Planets*.

Burton J. A., Prim R. C., and Slichter W. P. (1953) The distribution of solute in crystals grown from the melt. Part I. Theoretical. *The journal of chemical physics*, 21: 1987-1991.
Čadek O., Souček O., Běhounková M., Choblet G., Tobie G., and Hron J. (2019) Long-term stability of Enceladus' uneven ice shell. *Icarus*, 319: 476-484.
Čadek O., Tobie G., Van Hoolst T., Massé M., Choblet G., Lefèvre A., Mitri G., Baland R. M., Běhounková M., Bourgeois O. and others. (2016) Enceladus's internal ocean and ice shell constrained from Cassini gravity, shape, and libration data. *Geophysical Research Letters*, 43: 5653-5660.
Carlson R., Anderson M., Mehlman R., and Johnson R. (2005) Distribution of hydrate on Europa: Further evidence for sulfuric acid hydrate. *Icarus*, 177: 461-471.
Cherepanov N. V. (1964) Structure of Sea Ice of Great Thickness. *Problems of Arctic Ice Research*, 267: 13-18.
Chyba C. F. (2000) Energy for microbial life on Europa. *Nature*, 403: 381-382.
Clarke D. B., and Ackley S. F. (1984) Sea ice structure and biological activity in the Antarctic marginal ice zone. *Journal of Geophysical Research: Oceans*, 89: 2087-2095.
Coriell S. R., McFadden G. B., and Sekerka R. F. (1985) Cellular growth during directional solidification. *Annual Review of Materials Science*, 15: 119-145.
Costa D., Sexstone G. A., Pomeroy J. W., Campbell D. H., Clow D. W., and Mast A. (2020) Preferential elution of ionic solutes in melting snowpacks: Improving process understanding through field observations and modeling in the Rocky Mountains. *Science of the Total Environment*, 710: 136273.
Council N. R. (2011) Vision and Voyages for Planetary Science in the Decade 2013-2022. The National Academies Press, Washington, DC.
Cox G. F. N., and Weeks W. F. (1975) Brine drainage and initial salt entrapment in sodium chloride ice.
Cox G. F. N., and Weeks W. F. (1988) Numerical simulations of the profile properties of undeformed first-year sea ice during the growth season. *Journal of Geophysical Research: Oceans*, 93: 12449-12460.
Craft K., and Roberts J. Fracture formation post impact on Enceladus?
Craft K. L., Patterson G. W., Lowell R. P., and Germanovich L. (2016) Fracturing and flow: Investigations on the formation of shallow water sills on Europa. *Icarus*, 274: 297-313.
Craven M., Allison I., Brand R., Elcheikh A., Hunter J., Hemer M., and Donoghue S. (2004) Initial borehole results from the Amery Ice Shelf hot-water drilling project. *Annals of Glaciology*, 39: 531-539(9).
Craven M., Allison I., Fricker H., and Warner R. (2009) Properties of a marine ice layer under the Amery Ice Shelf, East Antarctica. *Journal of Glaciology*, 55: 717-728(12).
Craw L. (2020) The Ice Shelf Lasagne: Understanding the Effects of Differing Rheologies on the Dynamics of an Ice Shelf, Abstract C015-07.AGU Fall Meeting.
Crawford G. D., and Stevenson D. J. (1988) Gas-driven water volcanism and the resurfacing of Europa. *Icarus*, 73: 66-79.
Daly M., Rack F., and Zook R. (2013) Edwardsiella andrillae, a new species of sea anemone from Antarctic Ice. *PloS one*, 8: e83476.
Daly S. F. (1984) Frazil Ice Dynamics. In: *CRREL Monograph*, U.S. Army Cold Regions Research and Engineering Laboratory, pp 56.
Daswani M. M., Vance S. D., Mayne M. J., and Glein C. R. (2021) A metamorphic origin for Europa's ocean. *Geophysical Research Letters*: e2021GL094143.

Davies T., Brimblecombe P., Tranter M., Tsiouris S., Vincent C., Abrahams P., and Blackwood I. (1987) The removal of soluble ions from melting snowpacks. In: *Seasonal snowcovers: physics, chemistry, hydrology*, Springer, pp 337-392.
Des Marais D. J., Nuth Iii J. A., Allamandola L. J., Boss A. P., Farmer J. D., Hoehler T. M., Jakosky B. M., Meadows V. S., Pohorille A., and Runnegar B. (2008) The NASA astrobiology roadmap. *Astrobiology*, 8: 715-730.
Dierckx M., and Tison J. L. (2013) Marine ice deformation experiments: an empirical validation of creep parameters. *Geophysical research letters*, 40: 134-138.
Drebushchak V. A., Drebushchak T. N., Ogienko A. G., and Yunoshev A. S. (2019) Crystallization of sodium chloride dihydrate (hydrohalite). *Journal of Crystal Growth*, 517: 17-23.
Eicken H. (1992) Salinity profiles of Antarctic sea ice: Field data and model results. *Journal of Geophysical Research: Oceans*, 97: 15545-15557.
Eicken H. (1998) Antarctic Research Series. In: *Deriving Modes and Rates of Ice Growth in the Weddell Sea from Microstructural, Salinity, and Stable-Isotope Data*, pp 89-122.
Eicken H. (2003) From the microscopic, to the macroscopic, to the regional scale: growth, microstructure and properties of sea ice. *Sea ice: an introduction to its physics, chemistry, biology and geology*: 22-81.
Ettema R., Karim M. F., and Kennedy J. F. (1984) Laboratory experiments on frazil ice growth in supercooled water. *Cold Regions Science and Technology*, 10: 43-58.
Ewert M., and Deming J. W. (2013) Sea ice microorganisms: Environmental constraints and extracellular responses. *Biology*, 2: 603-628.
Feistel R., and Wagner W. (2006) A new equation of state for H 2 O ice Ih. *Journal of Physical and Chemical Reference Data*, 35: 1021-1047.
Fischer P. D., Brown M. E., and Hand K. P. (2015) Spatially resolved spectroscopy of Europa: The distinct spectrum of large-scale chaos. *The Astronomical Journal*, 150: 164.
Fitzsimons S., Mager S., Frew R., Clifford A., and Wilson G. (2012) Formation of ice-shelf moraines by accretion of sea water and marine sediment at the southern margin of the McMurdo Ice Shelf, Antarctica. *Annals of Glaciology*, 53: 211-220(10).
Foldvik A., and Kvinge T. Conditional instability of sea water at the freezing point. 21: 169-174.
Fox-Powell M. G., and Cousins C. R. (2021) Partitioning of Crystalline and Amorphous Phases During Freezing of Simulated Enceladus Ocean Fluids. *Journal of Geophysical Research: Planets*, 126: e2020JE006628.
Fox-Powell M. G., Hallsworth J. E., Cousins C. R., and Cockell C. S. (2016) Ionic strength is a barrier to the habitability of Mars. *Astrobiology*, 16: 427-442.
Gaidos E. J., and Nimmo F. (2000) Tectonics and water on Europa. *Nature*, 405: 637-637.
Garrison D. L., Ackley S. F., and Buck K. R. (1983) A physical mechanism for establishing algal populations in frazil ice. *Nature*, 306: 363-365.
Garrison D. L., Close A. R., and Reimnitz E. (1989) Algae concentrated by frazil ice: evidence from laboratory experiments and field measurements. *Antarctic Science*, 1: 313-316.
Geissler P. E., Greenberg R., Hoppa G., Helfenstein P., McEwen A., Pappalardo R., Tufts R., Ockert-Bell M., Sullivan R., Greeley R. and others. (1998) Evidence for non-synchronous rotation of Europa. *Nature*, 391: 34869.
Gjessing Y., Hanssen-Bauer I., Fujii Y., Kameda T., Kamiyama K., and Kawamura T. (1993) Chemical Fractionation in Sea Ice and Glacier Ice. *Bulletin of Glacier Research*: 1-8.

Glein C., Postberg F., and Vance S. (2018) The geochemistry of enceladus: composition and controls. *Enceladus and the Icy Moons of Saturn*, 39.
Glein C. R., Baross J. A., and Waite Jr J. H. (2015) The pH of Enceladus' ocean. *Geochimica et Cosmochimica Acta*, 162: 202-219.
Golden K. M., Ackley S. F., and Lytle V. I. (1998) The Percolation Phase Transition in Sea Ice. *Science*, 282: 2238-2241.
Golden K. M., Eicken H., Heaton A. L., Miner J., Pringle D. J., and Zhu J. (2007) Thermal evolution of permeability and microstructure in sea ice. *Geophysical Research Letters*, 34.
Goodman J. C. (2018) Interactions Between Ocean Circulation and Topography in Icy Worlds. *LPICo*, 2085: 6048.
Gow A. J., and Epstein S. (1972) On the use of stable isotopes to trace the origins of ice in a floating ice tongue. *Journal of Geophysical Research*, 77: 6552-6557.
Gow A. J., and Langston D. (1977) Growth history of lake ice in relation to its stratigraphic, crystalline and mechanical structure. U.S. Army Cold Regions Research and Engineering Laboratory.
Granskog M. A., Uusikivi J., Sequeiros A. B., and Sonninen E. (2006) Relation of ice growth rate to salt segregation during freezing of low-salinity sea water (Bothnian Bay, Baltic Sea). *Annals of Glaciology*, 44: 134-138.
Granskog M. A., Virkkunen K., Thomas D. N., Ehn J., Kola H., and Martma T. (2004) Chemical properties of brackish water ice in the Bothnian Bay, the Baltic Sea. *Journal of Glaciology*, 50: 292-302.
Greeley R., Sullivan R., Coon M. D., Geissler P. E., Tufts B. R., Head J. W., Pappalardo R. T., and Moore J. M. (1998) Terrestrial Sea Ice Morphology: Considerations for Europa. *Icarus*, 135: 25-40.
Green A., Montesi L., and Cooper C. (2021) The Growth of Europa's Icy Shell: Convection and Crystallization. *Journal of Geophysical Research: Planets*, 126: e2020JE006677.
Greenberg R., Geissler P., Hoppa G., Tufts B. R., Durda D. D., Pappalardo R., Head J. W., Greeley R., Sullivan R., and Carr M. H. (1998) Tectonic Processes on Europa: Tidal Stresses, Mechanical Response, and Visible Features. *Icarus*, 135: 64-78.
Greene C. A., Gwyther D. E., and Blankenship D. D. (2017) Antarctic mapping tools for MATLAB. *Computers & Geosciences*, 104: 151-157.
Griewank P. J., and Notz D. (2013) Insights into brine dynamics and sea ice desalination from a 1-D model study of gravity drainage. *Journal of Geophysical Research: Oceans*, 118: 3370-3386.
Gross G., Wong P., and Humes K. (1977) Concentration dependent solute redistribution at the ice–water phase boundary. III. Spontaneous convection. Chloride solutions. *The Journal of Chemical Physics*, 67: 5264-5274.
Grothe S., Hughes K., and Langhorne P. (2014) 22nd IAHR International Symposium on Ice.
Hallsworth J. E., Yakimov M. M., Golyshin P. N., Gillion J. L. M., D'Auria G., de Lima Alves F., La Cono V., Genovese M., McKew B. A., and Hayes S. L. (2007) Limits of life in MgCl2-containing environments: chaotropicity defines the window. *Environmental Microbiology*, 9: 801-813.
Hammond N. P. (2020) Estimating the Magnitude of Cyclic Slip on Strike-Slip faults on Europa. *Journal of Geophysical Research: Planets*, 125: no-no.

1371 Hammond N. P., Parmenteir E. M., and Barr A. C. (2018) Compaction and Melt Transport in
1372 Ammonia-Rich Ice Shells: Implications for the Evolution of Triton. *Journal of*
1373 *Geophysical Research: Planets*, 123: 3105-3118.
1374 Hand K., and Carlson R. (2015) Europa's surface color suggests an ocean rich with sodium
1375 chloride. *Geophysical Research Letters*, 42: 3174-3178.
1376 Hand K. P., and Chyba C. F. (2007) Empirical constraints on the salinity of the europan ocean
1377 and implications for a thin ice shell. *Icarus*, 189: 424-438.
1378 Harrison J. D., and Tiller W. A. (1963) Ice interface morphology and texture developed during
1379 freezing. *Journal of Applied Physics*, 34: 3349-3355.
1380 Helfenstein P., and Parmentier E. M. (1985) Patterns of fracture and tidal stresses due to
1381 nonsynchronous rotation: Implications for fracturing on Europa. *Icarus*, 61: 175-184.
1382 Hemingway D. J., and Mittal T. (2019) Enceladus's ice shell structure as a window on internal
1383 heat production. *Icarus*, 332: 111-131.
1384 Hemingway D. J., Rudolph M. L., and Manga M. (2020) Cascading parallel fractures on
1385 Enceladus. *Nature Astronomy*, 4: 234-239.
1386 Hendrix A. R., Hurford T. A., Barge L. M., Bland M. T., Bowman J. S., Brinckerhoff W., Buratti
1387 B. J., Cable M. L., Castillo-Rogez J., and Collins G. C. (2019) The NASA roadmap to
1388 ocean worlds. *Astrobiology*, 19: 1-27.
1389 Hesse M. A., Jordan J. S., Vance S. D., and McCarthy C. (2020) Oxidant Transport Through
1390 Europa's Ice Shell by Brine Drainage from Chaotic Terrains. *LPI*: 3073.
1391 Holland P. R., Corr H. F. J., Vaughan D. G., Jenkins A., and Skvarca P. (2009) Marine ice in
1392 Larsen Ice Shelf. *Geophysical Research Letters*, 36.
1393 Hoppa G. (1999) Strike–Slip Faults on Europa: Global Shear Patterns Driven by Tidal Stress.
1394 *Icarus*, 141: 287-298.
1395 Hoppa G., Greenberg R., Tufts B. R., Geissler P., Phillips C., and Milazzo M. (2000)
1396 Distribution of strike-slip faults on Europa. *Journal of Geophysical Research: Planets*,
1397 105: 22617-22627.
1398 Hoppmann M., Richter M. E., Smith I. J., Jendersie S., Langhorne P. J., Thomas D. N., and
1399 Dieckmann G. (2020) Platelet ice, the Southern Ocean's hidden ice: a review. *Annals of*
1400 *Glaciology*, 62.
1401 Howell S. M. (2021) The Likely Thickness of Europa's Icy Shell. *The Planetary Science*
1402 *Journal*, 2: 129.
1403 Howell S. M., and Pappalardo R. T. (2018) Band Formation and Ocean-Surface Interaction on
1404 Europa and Ganymede. *Geophysical Research Letters*, 45: 4701-4709.
1405 Hsu H.-W., Postberg F., Sekine Y., Shibuya T., Kempf S., Horányi M., Juhász A., Altobelli N.,
1406 Suzuki K., and Masaki Y. (2015) Ongoing hydrothermal activities within Enceladus.
1407 *Nature*, 519: 207-210.
1408 Hunke E. C., Notz D., Turner A. K., and Vancoppenolle M. (2011) The multiphase physics of
1409 sea ice: A review. *Cryosphere*, 5: 989-1009.
1410 Hurford T. A., Helfenstein P., Hoppa G. V., Greenberg R., and Bills B. G. (2007) Eruptions
1411 arising from tidally controlled periodic openings of rifts on Enceladus. *Nature*, 447: 292-
1412 294.
1413 Iess L., Stevenson D. J., Parisi M., Hemingway D., Jacobson R. A., Lunine J. I., Nimmo F.,
1414 Armstrong J. W., Asmar S. W., and Ducci M. (2014) The gravity field and interior
1415 structure of Enceladus. *Science*, 344: 78-80.

Jackson K. A. (2004) Constitutional supercooling surface roughening. *Journal of Crystal Growth*, 264: 519-529.

Jansen D., Luckman A., Kulessa B., Holland P. R., and King E. C. (2013) Marine ice formation in a suture zone on the Larsen C Ice Shelf and its influence on ice shelf dynamics. *Journal of Geophysical Research: Earth Surface*, 118: 1628-1640.

Jia X., Kivelson M. G., Khurana K. K., and Kurth W. S. (2018) Evidence of a plume on Europa from Galileo magnetic and plasma wave signatures. *Nature Astronomy*, 2: 459-464.

Johnston S. A., and Montési L. G. J. (2017) The impact of a pressurized regional sea or global ocean on stresses on Enceladus. *Journal of Geophysical Research: Planets*, 122: 1258-1275.

Kalousová K., Souček O., Tobie G., Choblet G., and Čadek O. (2014) Ice melting and downward transport of meltwater by two-phase flow in Europa's ice shell. *Journal of Geophysical Research: Planets*, 119: 532-549.

Kamata S., and Nimmo F. (2017) Interior thermal state of Enceladus inferred from the viscoelastic state of the ice shell. *Icarus*, 284: 387-393.

Kang W., Mittal T., Bire S., Campin J.-M., and Marshall J. (2021) How does salinity shape ocean circulation and ice geometry on Enceladus and other icy satellites? *arXiv preprint arXiv:2104.07008*.

Kargel J. S., Kaye J. Z., Head Iii J. W., Marion G. M., Sassen R., Crowley J. K., Ballesteros O. P., Grant S. A., and Hogenboom D. L. (2000) Europa's crust and ocean: origin, composition, and the prospects for life. *Icarus*, 148: 226-265.

Khazendar A., and Jenkins A. (2003) A model of marine ice formation within Antarctic ice shelf rifts. *Journal of Geophysical Research*, 108.

Khazendar A., Rignot E., and Larour E. (2009) Roles of marine ice, rheology, and fracture in the flow and stability of the Brunt/Stancomb-Wills Ice Shelf. *Journal of Geophysical Research: Earth Surface*, 114.

Khazendar A., Tison J. L., Stenni B., Dini M., and Bondesan A. (2001) Significant marine-ice accumulation in the ablation zone beneath an Antarctic ice shelf. *Journal of Glaciology*, 47: 359-368.

Kite E. S., and Rubin A. M. (2016) Sustained eruptions on Enceladus explained by turbulent dissipation in tiger stripes. *Proceedings of the National Academy of Sciences*, 113: 3972-3975.

Koch I., Fitzsimons S., Samyn D., and Tison J.-L. (2015) Marine ice recycling at the southern McMurdo Ice Shelf, Antarctica. *Journal of Glaciology*, 61: 689-701(13).

Krembs C., Eicken H., and Deming J. W. (2011) Exopolymer alteration of physical properties of sea ice and implications for ice habitability and biogeochemistry in a warmer Arctic. *Proceedings of the National Academy of Sciences*, 108: 3653-3658.

Kulessa B., Jansen D., Luckman A. J., King E. C., and Sammonds P. R. (2014) Marine ice regulates the future stability of a large Antarctic ice shelf. *Nature communications*, 5: 1-7.

Kvajić G., and Brajović V. (1971) Anisotropic segregation of (K+) by dendritic ice crystals. *Journal of Crystal Growth*, 11: 73-76.

Langhorne P. J., and Robinson W. H. (1986) Alignment of crystals in sea ice due to fluid motion. *Cold Regions Science and Technology*, 12: 197-214.

Lee S., Pappalardo R. T., and Makris N. C. (2005) Mechanics of tidally driven fractures in Europa's ice shell. *Icarus*, 177: 367-379.

Legendre L., Aota M., Shirasawa K., Martineau M.-J., and Ishikawa M. (1991) Crystallographic structure of sea ice along a salinity gradient and environmental control of microalgae in the brine cells. *Journal of Marine Systems*, 2: 347-357.

Leliwa-Kopystyński J., Maruyama M., and Nakajima T. (2002) The water–ammonia phase diagram up to 300 MPa: Application to icy satellites. *Icarus*, 159: 518-528.

Leppäranta M. (2015) Structure and Properties of Lake Ice. In: *Freezing of Lakes and the Evolution of their Ice Cover*. edited by M Leppärantas, Springer Berlin Heidelberg, Berlin, Heidelberg, pp 51-90.

Lewis E. L., and Perkin R. G. (1981) The Practical Salinity Scale 1978: conversion of existing data. *Deep Sea Research Part A. Oceanographic Research Papers*, 28: 307-328.

Lewis E. L., and Perkin R. G. (1986) Ice pumps and their rates. *Journal of Geophysical Research: Oceans (1978–2012)*, 91: 11756-11762.

Lipenkov V. Y., Polyakova E., and Ekaykin A. (2015) Regularities of congelation ice development in subglacial Lake Vostok. *Ice and Snow*, 52: 65-77.

Lobo A. H., Thompson A. F., Vance S. D., and Tharimena S. (2021) A pole-to-equator ocean overturning circulation on Enceladus. *Nature Geoscience*, 14: 185-189.

Lofgren G., and Weeks W. F. (1969) Effect of growth parameters on substructure spacing in NaCl ice crystals. *journal of Glaciology*, 8: 153-164.

Loose B., Miller L. A., Elliott S., and Papakyriakou T. (2011) Sea ice biogeochemistry and material transport across the frozen interface. *Oceanography*, 24: 202-218.

Mager S. M., Smith I. J., Kempema E. W., Thomson B. J., and Leonard G. H. (2013) Anchor ice in polar oceans. *Progress in Physical Geography*, 37: 468-483.

Manga M., and Wang C. Y. (2007) Pressurized oceans and the eruption of liquid water on Europa and Enceladus. *Geophysical Research Letters*, 34.

Martin A., and McMinn A. (2018) Sea ice, extremophiles and life on extra-terrestrial ocean worlds. *International Journal of Astrobiology*, 17: 1-16.

Maus S. (2006) The planar-cellular transition during freezing of natural waters.11th International Conference on the Physics and Chemistry of Ice.

Maus S. (2007) On brine entrapment in sea ice: morphological stability, microstructure and convection. Logos-Verlag.

Maus S. (2020) The plate spacing of sea ice. *Annals of Glaciology*, 82.

Maus S., Müller S., Büttner J., Brütsch S., Huthwelker T., Schwikowski M., Enzmann F., and Vähätolo A. (2011) Ion fractionation in young sea ice from Kongsfjorden, Svalbard. *Annals of Glaciology*, 52: 301-310.

McCord T., Hansen G., Fanale F., Carlson R., Matson D., Johnson T., Smythe W., Crowley J., Martin P., and Ocampo A. (1998) Salts on Europa's surface detected by Galileo's near infrared mapping spectrometer. *Science*, 280: 1242-1245.

McCord T. B., Hansen G. B., Matson D. L., Johnson T. V., Crowley J. K., Fanale F. P., Carlson R. W., Smythe W. D., Martin P. D., and Hibbitts C. A. (1999) Hydrated salt minerals on Europa's surface from the Galileo near-infrared mapping spectrometer (NIMS) investigation. *Journal of Geophysical Research: Planets*, 104: 11827-11851.

McCord T. B., Teeter G., Hansen G. B., Sieger M. T., and Orlando T. M. (2002) Brines exposed to Europa surface conditions. *Journal of Geophysical Research: Planets*, 107: 4-1-4-6.

McGrath D., Steffen K., Holland P. R., Scambos T., Rajaram H., Abdalati W., and Rignot E. (2014) The structure and effect of suture zones in the Larsen C Ice Shelf, Antarctica. *Journal of Geophysical Research: Earth Surface*, 119: 588-602.

McKinnon W. B. (2015) Effect of Enceladus's rapid synchronous spin on interpretation of Cassini gravity. *Geophysical Research Letters*, 42: 2137-2143.
Meese D. A. (1989) The chemical and structural properties of sea ice in the southern Beaufort Sea. In: *CRREL Report*, U.S. Army Cold Regions Research and Engineering Laboratory, pp 144.
Melnikov I. (1995) An in situ experimental study of young sea ice formation on an Antarctic lead. *Journal of Geophysical Research: Oceans*, 100: 4673-4680.
Michaut C., and Manga M. (2014) Domes, pits, and small chaos on Europa produced by water sills. *Journal of Geophysical Research: Planets*, 119: 550-573.
Mitri G., and Showman A. P. (2005) Convective–conductive transitions and sensitivity of a convecting ice shell to perturbations in heat flux and tidal-heating rate: Implications for Europa. *Icarus*, 177: 447-460.
Moore J. C., Reid A. P., and Kipfstuhl J. (1994) Microstructure and electrical properties of marine ice and its relationship to meteoric ice and sea ice. *Journal of Geophysical Research: Oceans (1978–2012)*, 99: 5171-5180.
Morgan V. I. (1972) Oxygen Isotope Evidence for Bottom Freezing on the Amery Ice Shelf. *Nature*, 238: 393-394.
Mullins W. W., and Sekerka R. F. (1964) Stability of a planar interface during solidification of a dilute binary alloy. *Journal of applied physics*, 35: 444-451.
Nagashima K., and Furukawa Y. (1997) Solute distribution in front of an ice/water interface during directional growth of ice crystals and its relationship to interfacial patterns. *The Journal of Physical Chemistry B*, 101: 6174-6176.
Nakawo M., and Sinha N. K. (1981) Growth Rate and Salinity Profile of First-Year Sea Ice in the High Arctic. *Journal of Glaciology*, 27: 315-330.
Neal C. S. (1979) The Dynamics of the Ross Ice Shelf Revealed by Radio Echo-Sounding. *Journal of Glaciology*, 24: 295-307.
Nimmo F. (2004a) Non-Newtonian topographic relaxation on Europa. *Icarus*, 168: 205-208.
Nimmo F. (2004b) Stresses generated in cooling viscoelastic ice shells: Application to Europa. *Journal of Geophysical Research: Planets*, 109.
Nimmo F., and Bills B. G. (2010) Shell thickness variations and the long-wavelength topography of Titan. *Icarus*, 208: 896-904.
Nimmo F., and Gaidos E. (2002) Strike-slip motion and double ridge formation on Europa. *Journal of Geophysical Research: Planets*, 107: 5-1-5-8.
Nimmo F., Thomas P. C., Pappalardo R. T., and Moore W. B. (2007) The global shape of Europa: Constraints on lateral shell thickness variations. *Icarus*, 191: 183-192.
Notz D., and Worster M. G. (2009) Desalination processes of sea ice revisited. *Journal of Geophysical Research*, 114.
Oerter H., Kipfstuhl J., Determann J., Miller H., Wagenbach D., Minikin A., and Graft W. (1992) Evidence for basal marine ice in the Filchner–Ronne ice shelf. *Nature*, 358: 358399a0.
Ojakangas G., and Stevenson D. (1989) Thermal state of an ice shell on Europa. *Icarus*, 81: 220-241.
Oren A. (2008) Microbial life at high salt concentrations: phylogenetic and metabolic diversity. *Saline systems*, 4: 2.
Oren A. (2013) Life in magnesium-and calcium-rich hypersaline environments: salt stress by chaotropic ions. In: *Polyextremophiles*, Springer, pp 215-232.

Osterkamp T. E. (1977) Frazil-Ice Nucleation by Mass-Exchange Processes at the Air-Water Interface. *Journal of Glaciology*, 19: 619-627.
Osterkamp T. E., and Weber A. H. (1970) Electrical phenomena accompanying the phase change of dilute KCl solutions into single crystals of ice. *Journal of Glaciology*, 9: 269-277.
Pappalardo R., Head J., Greeley R., Sullivan R., Pilcher C., Schubert G., Moore W., Carr M., Moore J., and Belton M. (1998) Geological evidence for solid-state convection in Europa's ice shell. *Nature*, 391: 365-368.
Pappalardo R. T., and Barr A. C. (2004) The origin of domes on Europa: The role of thermally induced compositional diapirism. *Geophysical Research Letters*, 31.
Patthoff D. A., Kattenhorn S. A., and Cooper C. M. (2019) Implications of nonsynchronous rotation on the deformational history and ice shell properties in the south polar terrain of Enceladus. *Icarus*, 321: 445-457.
Pattyn F., Matsuoka K., Callens D., Conway H., Depoorter M., Docquier D., Hubbard B., Samyn D., and Tison J. L. (2012) Melting and refreezing beneath Roi Baudouin Ice Shelf (East Antarctica) inferred from radar, GPS, and ice core data. *Journal of Geophysical Research: Earth Surface*, 117.
Peddinti D. A., and McNamara A. K. (2015) Material transport across Europa's ice shell. *Geophysical Research Letters*, 42: 4288-4293.
Peddinti D. A., and McNamara A. K. (2019) Dynamical investigation of a thickening ice-shell: Implications for the icy moon Europa. *Icarus*, 329: 251-269.
Petrich C., and Eicken H. (2017) Overview of sea ice growth and properties. In: *Sea Ice*. edited by DN Thomass, John Wiley & Sons, pp 1-41.
Petrich C., Langhorne P., and Eicken H. (2011) Modeled Bulk Salinity of Growing First-Year Sea Ice and Implications for Ice Properties in Spring.International Conference on Port and Ocean Engineering under Arctic Conditions, Montreal, Canada.
Petrich C., Langhorne P. J., and Sun Z. F. (2006) Modelling the interrelationships between permeability, effective porosity and total porosity in sea ice. *Cold Regions Science and Technology*, 44: 131-144.
Pillay V., Gärtner R. S., Himawan C., Seckler M. M., Lewis A. E., and Witkamp G.-J. (2005) MgSO4+ H2O System at Eutectic Conditions and Thermodynamic Solubility Products of MgSO4⊙ 12H2O (s) and MgSO4⊙ 7H2O (s). *Journal of Chemical & Engineering Data*, 50: 551-555.
Pontefract A., Zhu T. F., Walker V. K., Hepburn H., Lui C., Zuber M. T., Ruvkun G., and Carr C. E. (2017) Microbial diversity in a hypersaline sulfate lake: a terrestrial analog of ancient Mars. *Frontiers in microbiology*, 8: 1819.
Postberg F., Clark R. N., Hansen C. J., Coates A. J., Dalle Ore C. M., Scipioni F., Hedman M. M., and Waite J. H. (2018) Plume and surface composition of Enceladus. *Enceladus and the Icy Moons of Saturn*: 129-162.
Postberg F., Kempf S., Schmidt J., Brilliantov N., Beinsen A., Abel B., Buck U., and Srama R. (2009) Sodium salts in E-ring ice grains from an ocean below the surface of Enceladus. *Nature*, 459: 1098-1101.
Postberg F., Schmidt J., Hillier J., Kempf S., and Srama R. (2011) A salt-water reservoir as the source of a compositionally stratified plume on Enceladus. *Nature*, 474: 620-2.
Price P. B. (2000) A habitat for psychrophiles in deep Antarctic ice. *Proceedings of the National Academy of Sciences*, 97: 1247-1251.

Price P. B. (2007) Microbial life in glacial ice and implications for a cold origin of life. *FEMS Microbiology Ecology*, 59: 217-231.
Price P. B. (2009) Microbial genesis, life and death in glacial ice. *Canadian journal of microbiology*, 55: 1-11.
Prockter L. M., Pappalardo R. T., and Head Iii J. W. (2000) Strike-slip duplexing on Jupiter's icy moon Europa. *Journal of Geophysical Research: Planets*, 105: 9483-9488.
Quick L. C., and Marsh B. D. (2015) Constraining the thickness of Europa's water–ice shell: insights from tidal dissipation and conductive cooling. *Icarus*, 253: 16-24.
Raymond J. A. (2011) Algal ice-binding proteins change the structure of sea ice. *Proceedings of the National Academy of Sciences*, 108: E198-E198.
Reeburgh W. S., and Springer-Young M. (1983) New measurements of sulfate and chlorinity in natural sea ice. *Journal of Geophysical Research: Oceans*, 88: 2959-2966.
Reimnitz E., Clayton J. R., Kempema E. W., Payne J. R., and Weber W. S. (1993) Interaction of rising frazil with suspended particles: tank experiments with applications to nature. *Cold Regions Science and Technology*, 21: 117-135.
Rhoden A. R., Hurford T. A., and Manga M. (2011) Strike-slip fault patterns on Europa: Obliquity or polar wander? *Icarus*, 211: 636-647.
Rhoden A. R., Wurman G., Huff E. M., Manga M., and Hurford T. A. (2012) Shell tectonics: A mechanical model for strike-slip displacement on Europa. *Icarus*, 218: 297-307.
Roberts D., Craven M., Cai M., Allison I., and Nash G. (2006) Protists in the marine ice of the Amery Ice Shelf, East Antarctica. *Polar Biology*, 30: 143-153.
Roberts J. H., and Nimmo F. (2008) Tidal heating and the long-term stability of a subsurface ocean on Enceladus. *Icarus*, 194: 675-689.
Robinson N. J., Grant B. S., Stevens C. L., Stewart C. L., and Williams M. J. M. (2019) Oceanographic observations in supercooled water: Protocols for mitigation of measurement errors in profiling and moored sampling. *Cold Regions Science and Technology*: 102954.
Rudolph M. L., and Manga M. (2009) Fracture penetration in planetary ice shells. *Icarus*, 199: 536-541.
Rutter J. W., and Chalmers B. (1953) A prismatic substructure formed during solidification of metals. *Canadian Journal of Physics*, 31: 15-39.
Schenk P., Matsuyama I., and Nimmo F. (2008) True polar wander on Europa from global-scale small-circle depressions. *Nature*, 453: 368.
Schilling N., Khurana K. K., and Kivelson M. G. (2004) Limits on an intrinsic dipole moment in Europa. *Journal of Geophysical Research: Planets (1991–2012)*, 109.
Schilling N., Neubauer F. M., and Saur J. (2007) Time-varying interaction of Europa with the jovian magnetosphere: Constraints on the conductivity of Europa's subsurface ocean. *Icarus*, 192: 41-55.
Schmidt B. E. (2020) The Astrobiology of Europa and the Jovian System. *Planetary Astrobiology*: 185.
Schmidt B. E., Blankenship D. D., Patterson G. W., and Schenk P. M. (2011) Active formation of 'chaos terrain' over shallow subsurface water on Europa. *Nature*, 479: 502.
Seidensticker R. G. (1972) Partitioning of HCl in the water-ice system. *The Journal of Chemical Physics*, 56: 2853-2857.
Sekerka R. F., Coriell S. R., and McFadden G. B. (2015) Morphological stability. In: *Handbook of Crystal Growth*, Elsevier, pp 595-630.

Shokr M., and Sinha N. (2015) Sea ice: physics and remote sensing. John Wiley & Sons.
Soderlund K. M. (2019) Ocean dynamics of outer solar system satellites. *Geophysical Research Letters*, 46: 8700-8710.
Soderlund K. M., Kalousová K., Buffo J. J., Glein C. R., Goodman J. C., Mitri G., Patterson G. W., Postberg F., Rovira-Navarro M., and Rückriemen T. (2020) Ice-Ocean Exchange Processes in the Jovian and Saturnian Satellites. *Space Science Reviews*, 216: 1-57.
Soderlund K. M., Schmidt B. E., Wicht J., and Blankenship D. D. (2013) Ocean-driven heating of Europa's icy shell at low latitudes. *Nature Geoscience*, 7: 16-19.
Sotin C., Head III J. W., and Tobie G. (2002) Europa: Tidal heating of upwelling thermal plumes and the origin of lenticulae and chaos melting. *Geophysical Research Letters*, 29: 74-1-74-4.
Souchez R., Meneghel M., Tison J. L., Lorrain R., Ronveaux D., Baroni C., Lozej A., Tabacco I., and Jouzel J. (1991) Ice composition evidence of marine ice transfer along the bottom of a small Antarctic Ice Shelf. *Geophysical Research Letters*, 18: 849-852.
Souchez R., Petit J.-R., Tison J.-L., Jouzel J., and Verbeke V. (2000) Ice formation in subglacial Lake Vostok, central Antarctica. *Earth and Planetary Science Letters*, 181: 529-538.
Souchez R., Petit J. R., Jouzel J., De Angelis M., and Tison J. L. (2004) Reassessing Lake Vostok's behaviour from existing and new ice core data. *Earth and Planetary Science Letters*, 217: 163-170.
Souchez R., Tison J. L., and Jouzel J. (1988) Deuterium concentration and growth rate of Antarctic first-year sea ice. *Geophysical research letters*, 15: 1385-1388.
Sparks W. B., Schmidt B. E., McGrath M. A., Hand K. P., Spencer J. R., Cracraft M., and Deustua S. E. (2017) Active cryovolcanism on Europa? *The Astrophysical Journal Letters*, 839: L18.
Spencer J., Nimmo F., Ingersoll A. P., Hurford T., Kite E., Rhoden A., Schmidt J., and Howett C. (2018) Plume origins and plumbing: from ocean to surface. *Enceladus and the Icy Moons of Saturn*: 163.
Spencer J. R., Pearl J. C., Segura M., Flasar F. M., Mamoutkine A., Romani P., Buratti B. J., Hendrix A. R., Spilker L. J., and Lopes R. M. C. (2006) Cassini Encounters Enceladus: Background and the Discovery of a South Polar Hot Spot. *Science*, 311: 1401-1405.
Squyres S. W., Reynolds R. T., Cassen P. M., and Peale S. J. (1983) The evolution of Enceladus. *Icarus*, 53: 319-331.
Steinbrügge G., Voigt J. R. C., Wolfenbarger N. S., Hamilton C. W., Soderlund K. M., Young D. A., Blankenship D. D., Vance S. D., and Schroeder D. M. (2020) Brine Migration and Impact-Induced Cryovolcanism on Europa. *Geophysical Research Letters*, 47: e2020GL090797.
Tajeddine R., Soderlund K. M., Thomas P. C., Helfenstein P., Hedman M. M., Burns J. A., and Schenk P. M. (2017) True polar wander of Enceladus from topographic data. *Icarus*, 295: 46-60.
Terwilliger J. P., and Dizio S. F. (1970) Salt rejection phenomena in the freezing of saline solutions. *Chemical Engineering Science*, 25: 1331-1349.
Thomas D. N. (2017) Sea ice. John Wiley & Sons.
Thomas E. C., Hodyss R., Vu T. H., Johnson P. V., and Choukroun M. (2017) Composition and evolution of frozen chloride brines under the surface conditions of Europa. *ACS Earth and Space Chemistry*, 1: 14-23.

Tison J. L., Khazendar A., and Roulin E. (2001) A two-phase approach to the simulation of the combined isotope/salinity signal of marine ice. *Journal of Geophysical Research: Oceans*, 106: 31387-31401.

Tison J. L., Lorrain R. D., Bouzette A., Dini M., Bondesan A., and StiéVenard M. (1998) Linking Landfast Sea Ice Variability to Marine Ice Accretion at Hells Gate Ice Shelf, Ross Sea. pp 375-407.

Tison J. L., Ronveaux D., and Lorrain R. D. (1993) Low salinity frazil ice generation at the base of a small Antarctic ice shelf. *Antarctic Science*, 5: 309-322.

Toner J. D., Catling D. C., and Light B. (2014) The formation of supercooled brines, viscous liquids, and low-temperature perchlorate glasses in aqueous solutions relevant to Mars. *Icarus*, 233: 36-47.

Tosca N. J., Knoll A. H., and McLennan S. M. (2008) Water activity and the challenge for life on early Mars. *Science*, 320: 1204-1207.

Trumbo S. K., Brown M. E., and Hand K. P. (2019) Sodium chloride on the surface of Europa. *Science advances*, 5: eaaw7123.

Tsiouris S., Vincent C. E., Davies T. D., and Brimblecombe P. (1985) The elution of ions through field and laboratory snowpacks. *Annals of Glaciology*, 7: 196-201.

Turtle E. P., and Pierazzo E. (2001) Thickness of a Europan ice shell from impact crater simulations. *Science*, 294: 1326-1328.

Vance S., and Goodman J. (2009) Oceanography of an ice-covered moon. *Europa*: 459-482.

Vance S. D., Barge L. M., Cardoso S., and Cartwright J. (2019) Self-Assembling Ice Membranes on Europa: Brinicle Properties, Field Examples, and Possible Energetic Systems in Icy Ocean Worlds. *Astrobiology*, 19: 685-695.

Vance S. D., Journaux B., Hesse M., and Steinbrügge G. (2021a) The Salty Secrets of Icy Ocean Worlds. *Journal of Geophysical Research: Planets*, 126: e2020JE006736.

Vance S. D., Styczinski M., Bills B., Cochrane C., Soderlund K., Gómez-Pérez N., and Paty C. (2021b) Magnetic induction responses of Jupiter's ocean moons including effects from adiabatic convection. *Journal of Geophysical Research: Planets*, 126: e2020JE006418.

Waite J. H., Glein C. R., Perryman R. S., Teolis B. D., Magee B. A., Miller G., Grimes J., Perry M. E., Miller K. E., and Bouquet A. (2017) Cassini finds molecular hydrogen in the Enceladus plume: evidence for hydrothermal processes. *Science*, 356: 155-159.

Waite J. H., Lewis W. S., Magee B. A., Lunine J. I., McKinnon W. B., Glein C. R., Mousis O., Young D. T., Brockwell T., Westlake J. and others. (2009) Liquid water on Enceladus from observations of ammonia and 40Ar in the plume. *Nature*, 460: 487-490.

Walker C. C., Bassis J. N., and Schmidt B. E. (2021) Propagation of Vertical Fractures through Planetary Ice Shells: The Role of Basal Fractures at the Ice–Ocean Interface and Proximal Cracks. *The Planetary Science Journal*, 2: 135.

Walker C. C., and Schmidt B. E. (2015) Ice collapse over trapped water bodies on Enceladus and Europa. *Geophysical Research Letters*, 42: 712-719.

Warren S. G., Roesler C. S., Morgan V. I., Brandt R. E., Goodwin I. D., and Allison I. (1993) Green icebergs formed by freezing of organic-rich seawater to the base of Antarctic ice shelves. *Journal of Geophysical Research: Oceans (1978–2012)*, 98: 6921-6928.

Weeks W. (2010) On sea ice. University of Alaska Press.

Weeks W. F., and Ackley S. F. (1986) The Growth, Structure, and Properties of Sea Ice. In: *CRREL Monograph*, U.S. Army Cold Regions Research and Engineering Laboratory, pp 9-164.

Weeks W. F., and Lofgren G. (1967) The effective solute distribution coefficient during the freezing of NaCl solutions. *Physics of snow and ice: Proceedings*, 1: 579-597.

Wells A. J., Hitchen J. R., and Parkinson J. R. G. (2019) Mushy-layer growth and convection, with application to sea ice. *Philosophical Transactions of the Royal Society A*, 377: 20180165.

Wettlaufer J. S. (1992) Directional Solidification of Salt Water: Deep and Shallow Cells. *Europhysics Letters (EPL)*, 19: 337-342.

Wettlaufer J. S. (1998) Introduction to crystallization phenomena in natural and artificial sea ice. *The Physics of ice covered seas, edited by: Lepparantä, M., Univ. of Helsinki, Helsinki*: 105-195.

Zeng Y., and Jansen M. F. (2021) Ocean Circulation on Enceladus with a High- versus Low-salinity Ocean. *The Planetary Science Journal*, 2: 151.

Zimmer C., Khurana K. K., and Kivelson M. G. (2000) Subsurface Oceans on Europa and Callisto: Constraints from Galileo Magnetometer Observations. *Icarus*, 147: 329-347.

Zolotov M. Y. (2007) An oceanic composition on early and today's Enceladus. *Geophysical Research Letters*, 34.

Zolotov M. Y. (2008) Oceanic composition on Europa: Constraints from mineral solubilities.Lunar and Planetary Science Conference.

Zolotov M. Y., and Kargel J. S. (2009) On the chemical composition of Europa's icy shell, ocean, and underlying rocks. University of Arizona Press Tucson, AZ.

Zolotov M. Y., and Shock E. L. (2001) Composition and stability of salts on the surface of Europa and their oceanic origin. *Journal of Geophysical Research: Planets (1991–2012)*, 106: 32815-32827.

Zotikov I. A., Zagorodnov V. S., and Raikovsky J. V. (1980) Core Drilling Through the Ross Ice Shelf (Antarctica) Confirmed Basal Freezing. *Science*, 207: 1463-1465.